

**The influence of surface canopy water on L-band backscatter from corn  
A study combining detailed In situ data and the Tor Vergata radiative transfer model**

Khabbazan, S.; Steele-Dunne, S. C.; Vermunt, P. C.; Guerriero, L.; Judge, J.

**DOI**

[10.1016/j.srs.2024.100137](https://doi.org/10.1016/j.srs.2024.100137)

**Publication date**

2024

**Document Version**

Final published version

**Published in**

Science of Remote Sensing

**Citation (APA)**

Khabbazan, S., Steele-Dunne, S. C., Vermunt, P. C., Guerriero, L., & Judge, J. (2024). The influence of surface canopy water on L-band backscatter from corn: A study combining detailed In situ data and the Tor Vergata radiative transfer model. *Science of Remote Sensing*, 9, Article 100137. <https://doi.org/10.1016/j.srs.2024.100137>

**Important note**

To cite this publication, please use the final published version (if applicable).  
Please check the document version above.

**Copyright**

Other than for strictly personal use, it is not permitted to download, forward or distribute the text or part of it, without the consent of the author(s) and/or copyright holder(s), unless the work is under an open content license such as Creative Commons.

**Takedown policy**

Please contact us and provide details if you believe this document breaches copyrights.  
We will remove access to the work immediately and investigate your claim.



# The influence of surface canopy water on L-band backscatter from corn: A study combining detailed *In situ* data and the Tor Vergata radiative transfer model

S. Khabbazan<sup>a,b,\*</sup>, S.C. Steele-Dunne<sup>a</sup>, P.C. Vermunt<sup>b,1</sup>, L. Guerriero<sup>c</sup>, J. Judge<sup>d</sup>

<sup>a</sup> Department of Geoscience and Remote Sensing, Faculty of Civil Engineering and Geosciences, Delft University of Technology (TU Delft), Stevinweg 1, Delft, 2628, CN, Netherlands

<sup>b</sup> Department of Water Management, Faculty of Civil Engineering and Geosciences, Delft University of Technology (TU Delft), Stevinweg 1, Delft, 2628, CN, Netherlands

<sup>c</sup> Department of Civil Engineering and Computer Science, Tor Vergata University, Rome, 00133, Italy

<sup>d</sup> Center for Remote Sensing, Department of Agricultural and Biological Engineering, University of Florida, Gainesville, FL, 32611, Florida, USA

## ARTICLE INFO

### Keywords:

Agriculture  
Radar  
Soil moisture  
Dew  
Interception

## ABSTRACT

The presence, duration, and amount of surface canopy water (SCW) is important in microwave remote sensing for agricultural applications. Our current understanding of the effect of SCW on total backscatter and the underlying mechanisms is limited. The aim of this study is to investigate the effect of SCW on backscatter as a function of frequency and polarization, and to understand the underlying mechanisms. For this purpose, the radiative transfer model developed at the Tor Vergata University was used to simulate the total backscatter at L-, C-, and X-band. First, simulations from the standard Tor Vergata model were compared to L-band observations. Then, two additional implementations of the model were developed to account for the effect of SCW and the presence of water on the soil surface on radar backscatter. Representing SCW by the inclusion of additional water in the vegetation leads to an increase in vegetation volume scattering and a reduction in the contribution from double bounce and direct scattering from the ground. This increases total backscatter, particularly at lower frequencies. Results suggest that the difference between backscatter in the presence and absence of SCW can be up to around 2.5 dB in L-band and likely less at higher frequencies. The effect of water on the canopy (SCW) reaches its maximum during the mid and late season as the crop reached its maximum biomass. The influence of dew on the reflectivity of the soil surface resulted in a difference of up to 3.8 dB between backscatter in the presence and absence of SCW. In particular, at low frequencies and low vegetation cover, the presence of water on the soil surface needs to be taken into account to correctly capture the sub-daily dynamics in backscatter. The findings of this study are relevant for current and future SAR missions including Sentinel-1, ROSE-L, NISAR, SAOCOM, ALOS, CosmoSkyMed, TerraSAR-X, TanDEM-X and constellations such as those of ICEYE, and Capella which have dawn/dusk overpasses or multiple overpasses per day.

## 1. Introduction

Surface canopy water (SCW) refers to water present in the form of dew or interception from irrigation or precipitation on the canopy surface. Several studies have investigated the influence of the presence of water on the canopy surface. It has been shown that the presence of SCW is instrumental in the restoration of water content in plants following significant dehydration. Moreover, SCW serves as a vital moisture

provider for vegetation in dry regions. Particularly during the arid season, SCW can play an important role in the recovery of the water content in plants after heavy water loss (Willis, 1984; Agam and Berliner, 2006). Additionally, SCW can be beneficial for crops by reducing the local (near-leaf) vapor pressure deficit, thereby facilitating stomatal activity and photosynthesis (Gerlein-Safdi et al., 2018; Agam and Berliner, 2006; Dawson and Goldsmith, 2018). Dew formation and its accumulation on soil surfaces can serve to recharge soil moisture and

\* Corresponding author. Department of Geoscience and Remote Sensing, Faculty of Civil Engineering and Geosciences, Delft University of Technology (TU Delft), Stevinweg 1, Delft, 2628, CN, Netherlands.

E-mail addresses: [s.khabbazan@tudelft.nl](mailto:s.khabbazan@tudelft.nl), [saeed.khabbazan@gmail.com](mailto:saeed.khabbazan@gmail.com) (S. Khabbazan).

<sup>1</sup> Now at Faculty of Geo-Information Science and Earth Observation (ITC), University of Twente.

<https://doi.org/10.1016/j.srs.2024.100137>

Received 25 August 2023; Received in revised form 2 May 2024; Accepted 12 May 2024

Available online 15 May 2024

2666-0172/© 2024 The Authors. Published by Elsevier B.V. This is an open access article under the CC BY license (<http://creativecommons.org/licenses/by/4.0/>).

mitigate soil layer evaporation if the moisture is not evaporated before it can infiltrate (De Jeu et al., 2004). On the other hand, leaf wetness can contribute to the development of diseases in many crops (Huber and Gillespie, 1992; Agam and Berliner, 2006; Kabela et al., 2009). The duration and amount of SCW can influence fungal diseases, expansion of bacteria and fungal pathogens, and germination of spores on many crops (Huber and Gillespie, 1992). Therefore, information about the duration and amount of SCW can be valuable to support crop management decisions such as the optimal scheduling of fungicide applications.

In addition to the direct effect of SCW on hydrology and plant biology, SCW can directly affect microwave observations and influence the retrieval and estimation of soil moisture, vegetation optical depth (VOD), biophysical variables, canopy fuel load, and crop classification (Wood et al., 2002; Riedel and Schmullius, 2003a,b; Kabela et al., 2009; Hornbuckle et al., 2010; Tanase et al., 2015; Heffernan and Strimbu, 2021; Khabbazan et al., 2021a, 2021b). During the Soil Moisture Experiment 2005 (SMEX05) field campaign, Kabela et al. (2009) examined the occurrence, length, quantity, and distribution of dew in both corn and soybean. The study observed that dew was present for over 80 percent of the days, specifically between 00:30 and 06:30 central standard time (CST), throughout the SMEX05 campaign. The findings revealed that the dew quantity ranged from approximately 0.01 to 0.6 mm in corn. Additionally, the spatial distribution of dew within the plant canopy showed variations during light, moderate, and heavy dew events.

Radar observations from agricultural land are highly sensitive to the dielectric and structural properties of the crops and soil depending on system properties such as frequency, polarization, and incidence angle (Judge et al., 2021; Steele-Dunne et al., 2017; McNairn and Shang, 2016; Liu et al., 2013). The presence of SCW increases the amount of water present in the vegetation layer above the soil. However, this water will be on the outside of the plant tissue. Therefore, it does not increase the water content of the plant tissue. Having a water layer on top of the canopy changes the radar signal scattering and absorption characteristics, resulting in an increased observed backscatter (Allen and Ulaby, 1984; Gillespie et al., 1990; Wood et al., 2002; Riedel and Schmullius, 2003a,b; Kabela et al., 2009; Hornbuckle et al., 2010).

Several experimental studies have been conducted using different radar configurations over different crop types to understand the effect of SCW on radar data. In an early study conducted by Gillespie et al. (1990) over a wheat field, it was found that radar backscatter increased by 4 dB in C-band and 1 dB in the L- and Ku-band during dew events. It was found that an incidence angle of 20° had the highest sensitivity to the presence of dew compared with incidence angles of 40 and 60°.

However, Herold et al. (2001) reported no significant effect from SCW on radar backscatter at X-band and a modest increase of up to 1 dB in C-band for forest and non-cereal crops such as corn and potato with heterogeneous surface structure. They found that L-band observations were less sensitive to SCW than C-band for all crop types.

A series of experiments conducted by Riedel et al. (2002) and Riedel and Schmullius (2003a,b); Riedel and Schmullius (2003a,b) used polarimetric data at L-, C-, and X-band from E-SAR over different crop types to investigate the effect of SCW on radar observations, scattering mechanisms, and crop classification. At L-band ( $f = 1.3$  GHz), they found that the effect of SCW was less dependent on plant structure and a strong influence of SCW was observed on cross-pol data while no impact was observed on VV-pol data. At C-band ( $f = 5.3$  GHz), they observed that the impact on backscatter depended on vegetation structure and growth stages. At X-band ( $f = 9.6$  GHz), no significant influence was observed from dew events. In the experiment carried out by Riedel and Schmullius (2003a,b) and Riedel et al. (2002), the impact of dew and interception was analyzed separately for volume, surface, and double-bounce scattering. For this purpose, the authors exploited polarimetric target decomposition. This decomposition relies on some assumptions and, therefore, the separation among scattering mechanisms is never perfect and, importantly, is affected by the presence of dew or SCW. They found

an increase of about 2 dB in volume scattering in cross-pol under wet conditions. They also found a significant decline of around 4 dB in surface scattering and double bounce in the presence of SCW. They reported that the impact of dew on the signal was independent of vegetation type. They found that classification accuracy increased as SCW amount decreased, and that crop separability was affected by SCW.

Wood et al. (2002), compared RADARSAT-1 data from ascending and descending passes to understand the effect of SCW on crop separability. They found that the difference in backscatter between ascending and descending passes was similar among various crop types and that C-band backscatter was on average 1.7–2.5 dB higher during the dawn acquisition (6 a.m.) compared to the dusk acquisition (6 p.m.). Contrary to Riedel and Schmullius (2003a,b), they concluded that the overall separability of crops remains unaffected by the selection of overpass time. However, the choice of overpass time should be given consideration in the retrieval of crop biophysical variables, as the presence of dew increases the radar backscatter during dawn acquisitions.

Recently, Khabbazan et al. (2021a), investigated the impact of SCW on radar backscatter and crop biophysical parameter retrieval using L-band radar data and detailed ground data. They found that SCW was typically present from midnight to 10 a.m. which increased the L-band backscatter by 2–3 dB. They demonstrated that SCW directly influenced the backscatter data and the relationship between backscatter and plant biophysical variables, suggesting that daily SCW patterns should be considered in retrievals. The presence of SCW led to higher VOD estimates, impacting vegetation water content estimation. However, this study was not able to fully explain the effects of SCW on polarization and total backscatter contributions due to limited understanding of how the presence of surface canopy water affects the various contributions to total backscatter and solely focused on L-band data. The availability of C-band SAR data from Sentinel-1, Radarsat Constellation Mission and the advent of Sentinel-NG, as well as the availability of X-band SAR data from TerraSAR-X and TanDEM-X and observations from ICEYE and CappellaSpace SAR constellations create many possibilities for monitoring vegetation, and specifically agricultural monitoring using higher frequency radar observations.

The aim of this study is to investigate the effect of SCW on backscatter as a function of frequency, polarization, and growth stage and to understand the influence of SCW on the contributions to total backscatter. The radiative transfer model developed at the Tor Vergata University is used to simulate the backscatter response as a function of frequency and polarization. The standard form of the Tor Vergata model does not consider the presence of SCW on leaves. Therefore, two additional implementations of the Tor Vergata model are considered in this study, whereby the standard model is adapted to account for the presence of water on the surface of the vegetation and soil by adjusting the leaves' internal water content and soil moisture respectively. The three implementations are first compared to L-band data from the UF-LARS scatterometer and ground data collected during an intensive field campaign over a maize field in Florida, USA in 2018 to explore the potential difference in sensitivity to SCW as a function of polarization. Backscatter is also simulated (though it can not be validated) at C-band and X-band to provide some insight into the effect of SCW at higher frequencies according to the model.

## 2. Data and methods

### 2.1. Experimental site

The data for this study were collected during a field campaign near Citra, Florida at the Plant Science Research and Education Unit (PSREU) of the University of Florida and the Institute of Food and Agricultural Sciences (UF|IFAS). The campaign started during the bare soil phase in early April 2018 and lasted roughly 70 days, until harvest in mid-June (Vermunt et al., 2020). Sweet corn was sown in sandy soil at a

planting density of 7.9 plants  $m^{-2}$  and with row spacing of 92.5 cm. During the early vegetative stages, controlled irrigation was applied several times from midnight to early morning using a center-pivot irrigation system. More detailed descriptions of the study site can be found in Vermunt et al. (2020) and Khabbazan et al. (2021a).

## 2.2. Field measurements

### 2.2.1. Surface canopy water

The measurement of the presence, frequency, duration, and amount of surface canopy water (SCW) was conducted using three dielectric leaf wetness sensors (Pythos31) (METER Group, 2021b), with readings taken every 15 min.

At the start of the season, these sensors were fixed to a wooden pole located between two rows. Once the corn plants matured and their stems became robust, the sensors were relocated and attached directly to one plant. As the plants grew, the sensors positions were adjusted to maintain a uniform distribution along the plants height, capturing the vertical distribution of water droplets within the canopy. Additionally, each sensor angle was aligned to mimic the orientation of the adjacent leaves.

The primary reading from these sensors is a voltage (expressed in mV) that corresponds to the dielectric constant of a region roughly 1 cm from the sensor upper surface (METER Group, 2021b). This dielectric constant is proportional to the water quantity on the surface of the sensor. The EM50 data logger (METER Group, 2019) then translates this voltage into a scale described as "counts."

The water mass ( $M_w$ ) deposited on the sensor surface (measured in  $g\ m^{-2}$ ) is computed using an empirical formula provided by the manufacturer (METER Group, 2021c) and Cobos (2013):

$$M_w = 1.54 \times \exp(5.8 \times 10^{-3} \times counts) \quad (1)$$

According to Vermunt et al. (2020), two assumptions were utilized to convert the water mass on the sensors into SCW. Initially, each corn leaf area ( $A_{Leaf}$ ) in  $m^2$  was determined from the leaf length ( $l$ ) and width ( $w$ ), based on the premise that corn leaves were elliptical:

$$A_{Leaf} = \frac{\pi}{4} \times l \times w \quad (2)$$

Subsequently, it was assumed that the wetness level on a leaf at any given height was equivalent to the wetness on the nearest sensor to that leaf. Consequently, SCW could be calculated as:

$$SCW = \rho_{plant} \times \sum_{i=1}^n A_{Leaf_i} \times M_{w_i} \quad (3)$$

Here, SCW is SCW per square meter of ground ( $kg\ m^{-2}$ ),  $\rho_{plant}$  is the average number of plants per square meter of ground,  $n$  represents the number of leaves per plant, and  $M_{w_i}$  refers to the water mass on the sensor closest to leaf  $i$  expressed in kilograms per square meter of leaf.

### 2.2.2. Soil data

Surface to root zone soil moisture was measured every 15 min using 10 Decagon EC-5 sensors (METER Group, 2021a) in two pits located 40 m apart at 5 different depths. These sensors have 5 cm prong length with a  $\sim 0.2$  L measurement volume. At each depth, the sensor is fully inserted with  $45^\circ$  orientation from the nadir into the soil layer. In this study, only the averaged measurement at 5 cm depth was used as surface soil moisture. A site-specific calibration was conducted before the installation of sensors. Soil samples from the field were brought to the laboratory and soil moisture was measured using EC-5 sensors and the gravimetric sampling method for saturated to dry soil. The goodness of fit for the linear regression between the two methods was 0.993, and the RMSE was  $0.028\ m^3\ m^{-3}$ .

In the time between planting and crop emergence, surface roughness was measured using a 2-m long grid board. Roughness profiles were gathered both along and perpendicular to the row direction, digitized at

intervals of 1 cm. These digitized profiles were then utilized to calculate the root mean square (RMS) height and correlation length ( $L$ ) using the exponential correlation function, following to the process describe in Jang et al. (2005). The averaged RMS height and correlation length derived from both directions were found to be 0.92 cm and 9.17 cm, respectively.

### 2.2.3. Vegetation data

The gravimetric water content ( $M_g$ ) and the mass of water of various corn components like leaves, stems, ears, tassels, and tillers were measured through pre-dawn destructive sampling three times a week during the growing season, resulting in 20 observations. Four sampling locations were chosen outside the radar footprint. At each sampling time, eight field representative samples were taken from the sampling area, packed in plastic bags, and taken to the nearby lab for immediate processing. For each of the 8 samples, the leaves, stems, ears, tassels, and tillers were separated and labeled. Any surface water present on the plant tissue was gently removed with paper towels. Constituents with the same labels were collected in paper bags and weighed to determine fresh biomass. This process was done as quickly as possible to minimize changes in the internal water content of plant constituents. Then, all samples were placed in an oven at  $60^\circ C$  for 4–8 days, depending on the growth stage, to dry completely. The dry samples were weighed again to compute VWC and  $M_g$ .

The calculation of gravimetric water content ( $M_g$ ) was performed using the following formula:

$$M_g = \frac{W_f - W_d}{W_f} \quad (4)$$

where  $W_f$  and  $W_d$  represent the average fresh and dry mass of total plant or plant component (leaf, stem) per plant, respectively.

It should be mentioned that in soil science, gravimetric water content is traditionally defined as the mass of water in a sample divided by its dry mass. However, in the analysis of microwave dielectric behavior in vegetation material, following Ulaby et al. (1981); Ulaby and El-Rayes (1987); Matzler (1994), the gravimetric water content of plant constituents is calculated differently, employing the fresh weight of the canopy instead of the dry weight, as represented in Equation (4). Additionally, it should be noted that the Tor Vergata model adopts this definition of gravimetric water content as an input for the gravimetric moisture of plant constituents. For measuring internal vegetation water content (VWC), we measured the total mass of water in the leaves, stems, ears and (total) vegetation per ground area.

In addition to the destructive sampling, detailed vegetation geometry measurements were conducted once a week on 4 representative samples, with 8–10 measurements in total during the growing season. As mentioned already, internal vegetation water content (VWC) of the plant constituents (leaves, stems, ears, tassels and tillers) were measured during pre-dawn destructive sampling three times per week during the growing season. Hourly destructive sampling of VWC, or  $M_g$  is prohibitively laborious and time-consuming (Vermunt et al., 2022a, 2022b). Therefore, hourly values for  $M_g$  and vegetation geometry measurements were estimated using linear interpolation (see Fig. S1 in the supplementary material).

More detailed descriptions about soil and vegetation data, along with further information, can be found in our existing works (Vermunt et al., 2020; Khabbazan et al., 2021b).

### 2.2.4. Ground-based radar observations

Backscatter observations ( $\sigma^0$ ) were collected using the University of Florida L-band Automated Radar System (UF-LARS). This system operates at a central frequency of 1.25 GHz (Nagarajan et al., 2013) and is designed to acquire data at four polarization combinations (VV, HH, VH, and HV) simultaneously using a dual-polarization horn antenna. It was mounted on a 14 m Genie manlift and scanned the field at a fixed incidence angle of  $40^\circ$ . The measurements of VH and HV were nominally

equal. Therefore, following previous studies (Liu et al., 2016), their average is used and referred to as the cross-polarized backscatter  $\sigma_{XP}^0$ .

The Single Target Calibration Technique (STCT) was used to calculate backscatter coefficient from the received signal and the overall uncertainty of UFLARS measurements was quantified to be 1.49 dB (Vermunt et al., 2020; Liu et al., 2016). Internal calibration was applied during each acquisition and a single-target calibration technique using a 1 m trihedral corner reflector was applied several times during the season. The ground range and azimuth resolutions were calculated from the 3 dB beam-width, which measured  $14.7^\circ$  in the E-plane and  $19.7^\circ$  in the H-plane. Consequently, the single-scan footprints for HH, VV, and cross-pol were found to be 40, 39.7, and  $29.1 \text{ m}^2$ , respectively (Nagarajan et al., 2013; Vermunt et al., 2020). The system was programmed to automatically acquire 32 measurements per day for most of the growing season. Comprehensive descriptions of both the observations and the specifics of the UF-LARS system are available in the cited works (Nagarajan et al., 2013; Vermunt et al., 2020; Khabbazan et al., 2021a).

It is worth noting that all the sampling areas and sensor installations were positioned outside, yet close to, the radar footprint. This arrangement ensured no interference with the signal and protected against alterations in roughness that could occur due to foot traffic.

### 2.3. Radiative transfer model

In this study, the two-layer model developed at the University of Rome, Tor Vergata (Bracaglia et al., 1995) specifically for corn was used, and is referred to as the “Tor Vergata model” throughout. This model has been used in multiple studies for the simulation of radar backscatter across various crop types and frequencies, ranging from P- to X-band (Ferrazzoli and Guerriero, 1995, 1996; Ferrazzoli et al., 1999a,b; Della Vecchia et al., 2004, 2006a,b; Blaes et al., 2006; Della Vecchia et al., 2007a, 2008; Guerriero et al., 2013; Stamenkovic et al.; Guerriero et al., 2016; Link et al., 2017; Acuña et al., 2019). The model has been validated at L-, C-, and X-band frequencies. In a study conducted by Della Vecchia et al. (2008), the model simulated corn scattering during the growth season across a frequency range of 2.5–10.2 GHz and incidence angles of  $20\text{--}50^\circ$  for all linear polarizations. This was compared with data from the tower based Radio ScAtteroMeter (RASAM). The findings indicated that the RMS error between the simulated and actual data across five different frequencies ranged from 1.37 to 2.23 dB. In another study, Della Vecchia et al. (2006a) employed the model for maize and wheat backscatter simulation at C-band frequencies, comparing it with ground-based and ERS-2 data. The model performance demonstrated RMSE of 1.44 and 0.96 dB when comparing simulated and observed data in corn fields, and 1.78 and 2.23 dB in wheat fields. The RMS errors of less than 2 dB in previous studies demonstrate the model performance matched observations, demonstrating its sensitivity to crop growth across various frequencies. Vermunt et al. (2020) leveraged the model to quantify the relative importance of soil and vegetation contributions to the total L-band backscatter of maize and how this changes during the growing season. Note that Vermunt et al. (2020) used the same observations from UF LARS. However, they were not able to account for the influence of surface canopy water (SCW) or the presence of water on top of the soil layer on backscatter or on the contributions to total backscatter.

This model is a discrete microwave scattering model based on radiative transfer theory. It is designed to simulate both the scattering and extinction properties of vegetation elements, as well as the underlying soil. This is achieved by applying the most suitable electromagnetic approximation, considering factors such as the shape of the scatterer and the wavelength. In this model, the cornfield is modeled as a homogeneous half-space with a single-layer rough interface, representing the soil. This interface is overlaid by another single layer made up of the stems, leaves, and petioles (ribs). This version of the model does not consider ears, as Della Vecchia et al. (2006a) discovered that including

them has a minimal impact on the total simulated backscatter from corn, with a change of less than 0.3 dB. The scattering coefficient for the single-layer soil is determined using the original formulation of the Integral Equation Model (IEM) (Fung et al., 1992). The required input parameters for this model include soil permittivity, and soil roughness factors like the root mean square (RMS) height (s), correlation length (l), and the exponential autocorrelation function. Baghdadi et al. (2004, 2006); Álvarez-Mozos et al. (2008) and others suggest calibrating the correlation length, selecting the value that yields the minimum RMSE between observed and simulated backscatter for the measured RMS height. This approach is generally a pragmatic solution to the difficulty in measuring accurate correlation length in the field. However, we measured both RMS height and correlation length (Section 2.2.2), and use the measured values directly here.

For the vegetation layer, leaves are represented by dielectric discs, while stems and ribs are represented by dielectric cylinders. The characteristics of the discs are described by their diameter and thickness, whereas the cylinders are defined by their diameter and length. Lengthy leaves are broken down into multiple discs, each with a diameter equivalent to the leaf width. The orientation of leaves and ribs scatterers within the canopy layer is arranged randomly assuming a uniform distribution.

To compute the scattering matrices and the extinction vector, different approximations are used depending on the frequency. For frequencies up to 5 GHz, the Rayleigh-Gans approximation (Eom and Fung, 1984) is used for both leaves and ribs (L-band). For frequencies higher than 5 GHz, the Physical Optics approximation is used for leaves and the infinite length approximation (Karam and Fung, 1988) is used for ribs (C- and X-band). For stems, the infinite length approximation is used for all frequencies. The model utilizes the matrix doubling algorithm (Eom and Fung, 1984) to combine contributions from the various scatterers, and between vegetation and soil. This method allows for the inclusion of multiple scattering effects of any order in the calculation of the backscattering coefficient and it can separate contributions of different scatterers in the vegetation canopy. In the Tor Vergata model, the total backscatter has four contributions:

$$\sigma_{total}^0 = \sigma_v^0 + \sigma_{vg}^0 + \sigma_{ab}^0 + \sigma_g^0 \quad (5)$$

where  $\sigma_{total}^0$  is the total backscatter coefficient,  $\sigma_v^0$  is the vegetation scattering (volume scattering by the vegetation layer),  $\sigma_{vg}^0$  is the vegetation-ground scattering (multiple scattering effects due to interactions between the vegetation and ground),  $\sigma_{ab}^0$  is the soil-stem double bounce specular reflection, and  $\sigma_g^0$  is the direct component solely from the soil surface attenuated by the canopy. In  $\sigma_{vg}^0$ , multiple interactions between the plant elements, and between the plant elements and the ground are considered, whereas in  $\sigma_{ab}^0$ , only the corner reflection between the vertical stem and the ground is taken into account, as illustrated in Fig. 1.

A more detailed and comprehensive description of the model and its assumptions can be found in Bracaglia et al. (1995). A list of the input variables provided to the Tor Vergata model is presented in Table 1.

### 2.4. Accounting for SCW in the Tor Vergata model

The presence of SCW increases the amount of water present in the vegetation layer above the soil. In reality, SCW consists of droplets of free water on the outside of the leaves. It is not trivial to introduce this into a model because it would require parameterization of the shape, size, and distribution of the water droplets and a model to account for their behavior in an electric field. As a first approximation, we account for the presence of water on the surface of the vegetation by adjusting the internal gravimetric water content for the disc and small cylinders so that the additional moisture due to SCW “appears” as extra leaf moisture. It implicitly assumes that water on the surface of the leaf behaves in the same way as water within the leaf, which may not be the case.

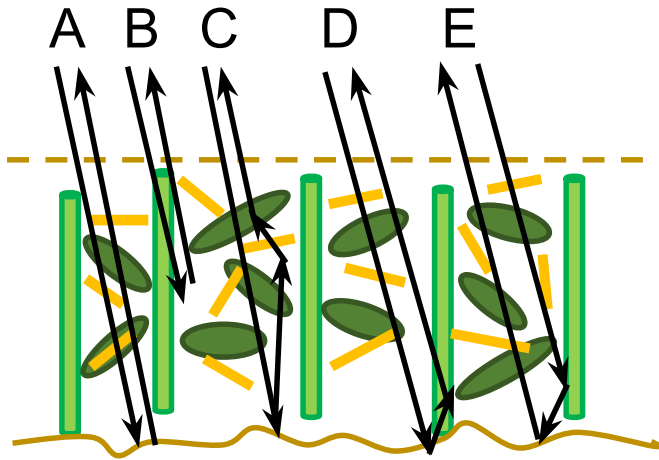


**Fig. 1.** Schematic representation of the radiative transfer model geometry for corn. The four components of rough soil, main stems, leaves, and ribs, and 5 scattering mechanisms of (A) direct soil ( $\sigma_g^0$ ), (B) vegetation ( $\sigma_v^0$ ), (C) ground-vegetation ( $\sigma_{vg}^0$ ), and (D, E) double bounce ( $\sigma_{db}^0$ ) are shown.

**Table 1**

List of input parameters for Tor Vergata model simulation (Vermunt et al., 2020).

Parameter	Value or Time series
Frequencies (GHz)	$L = 1.25/C = 5.405/X = 9.6$
Incidence angle (degree)	40
Soil volumetric moisture content	Time series
Soil RMS height (cm)	0.92
Soil correlation length (cm)	9.17
Plant density (plant $m^{-2}$ )	8
plant height (cm)	Time series
LAI	Time series
number of leaves per plant	Time series
Leaf area ( $cm^2$ )	Time series
Leaf half width (cm)	Time series
Disc (leaf) thickness (cm)	0.03
Disc (leaf) gravimetric moisture	Time series
Stem height	Time series
Stem radius	Time series
Stem gravimetric moisture	Time series
small cylinder (ribs) length (cm)	70% of leaf length
small cylinder (ribs) maximum radius (cm)	0–0.4
small cylinder (ribs) gravimetric moisture	Time series

Nonetheless, it at least includes the additional moisture, and ensures that it is distributed within the canopy using the canopy architecture. In the Tor Vergata model, the average gravimetric water content ( $M_g$ ) of all corn leaves is used as an input parameter for the disc (leaf) and small cylinders (ribs) gravimetric moisture to account for their internal water content. The adjusted internal gravimetric water content ( $M_{g+}$ ) for the disc and small cylinders is calculated as follows:

$$W_{f+leaf} = W_{fleaf} + \frac{SCW}{\rho_{plant}} \quad (6)$$

$$M_{g+} = \frac{W_{f+leaf} - W_{dleaf}}{W_{f+leaf}} \quad (7)$$

where  $W_{f+leaf}$  represents the aggregate mass of water within the corn leaves of one plant and the amount of SCW on the leaves of one plant, expressed in kilograms per plant.  $W_{fleaf}$  and  $W_{dleaf}$  represent the fresh and dry mass of corn leaves in one plant (kilograms per plant), respectively.

Vermunt et al. (2020) and Khabbazan et al. (2021a) observed increases in radar backscatter during the bare soil period that could not be explained by *in situ* soil moisture measurements at 5 cm but coincided with non-zero measurements of the SCW sensors. They argued that these increases could be attributed to the presence of a thin layer of dew visually observed on the soil surface. Here, we account for the effect of the presence of dew on the soil surface by setting the soil moisture in the surface layer to the measured saturated value for sandy soil ( $0.37 m^3 m^{-3}$ ) when the leaf wetness sensor indicates the presence of water.

In the following analysis, we will consider three implementations to investigate the effect of SCW on the vegetation and the soil surface:

- (1) In the “VWC” scenario, the presence of SCW is not taken into account and the measured  $M_g$  was used for disc and small cylinders. This corresponds to a standard implementation of the Tor Vergata model.
- (2) In the “VWC<sup>+</sup>” scenario, the internal water content is adjusted so that the gravimetric water content used in the model is  $M_g +$  calculated using Eq. (7). In this scenario, the role of dew on the soil surface is not considered.
- (3) In the “VWC + SM<sup>+</sup>” scenario, the internal water content is adjusted so that the gravimetric water content used in the model is  $M_g +$  calculated using Eq. (7). In addition, the surface soil layer is assumed to be saturated when the presence of SCW is detected. Note that during the bare soil/early vegetation periods, the presence of water on the soil was visually observed during sampling periods and coincided with periods when dew had formed on the LWS. In this study, only a yes/no condition is considered rather than inferring an amount from the LWS which was slightly above the ground, not in contact with the soil, and oriented to emulate the geometry of a leaf.

### 3. Results and discussions

#### 3.1. Field measurements

##### 3.1.1. Hydrometeorological data

Detailed descriptions of all field measurements are provided by Vermunt et al. (2020); Khabbazan et al. (2021a). For completeness, these data, particularly the soil moisture at 5 cm, precipitation, and irrigation data are summarized in the Supplementary Material.

##### 3.1.2. SCW data

Fig. 2 (a) illustrates that the average water mass ( $M_w$ ) deposited on the surface of the three leaf wetness sensors (LWS) due to dew was approximately one-third of that resulting from interception. In the early season, the water accumulation on the LWS and canopy was primarily due to dew and interception from irrigation, whereas, in the mid-season, it was predominantly from interception from frequent rain events. In the late season, dew was the main source of wetness.

The results from Fig. 2 (a) indicate variability in the water mass on the LWS caused by dew events during the early season, highlighting both moderate and high dew occurrences. For example, the dew event on 6 May was the heaviest of the season, resulting in a water deposition of  $0.125 kg m^{-2}$  on the LWS, while the following day event (7 May) led to only  $0.02 kg m^{-2}$ . In case of the interception events, early season irrigation resulted in lower water deposition on the LWS compared to the precipitation events during the mid and late seasons.

Fig. 2 (b) displays a time series of the surface canopy water (SCW) on the corn leaves, which is derived from the water mass data on the LWS (Fig. 2 (a)) by applying equations (2) and (3). The results show that the amount of SCW increased with biomass accumulation. During the early season, the SCW was relatively low for both dew and interception events, approximately  $0.04$  and  $0.09 kg m^{-2}$  respectively. This increased up to  $0.47$  and  $1.28 kg m^{-2}$  in the late season. Comparing results from Fig. 2 (a) and (b) for the early season reveals that although the water

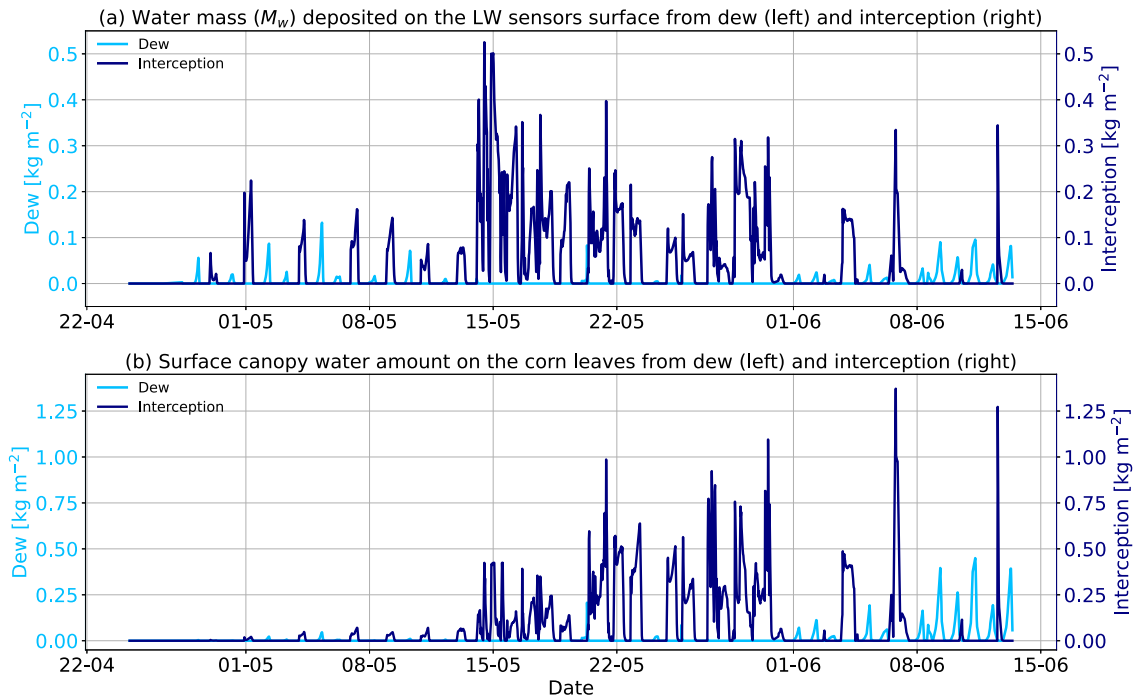


**Fig. 2.** Time series of (a) water mass ( $M_w$ ) deposited on the leaf wetness sensors surface in kg per square meter of leaf wetness sensor, and (b) the amount of estimate surface canopy water in kg of water per unit ground area.

mass on the LWS exhibited significant variation due to dew and irrigation, the SCW remained relatively consistent. This consistency in SCW can be attributed to the small size of the corn leaves during this period. As the corn reached its maximum biomass in the late season, the SCW increased by up to 10 times compared to the early season, even though the water mass on the LWS remained almost similar throughout. These results highlight the impact of biomass accumulation on the amount of water on top of the canopy surface.

The frequency of the presence of SCW is shown in Fig. S2 (supplementary material). SCW was present on more than 80 % of days after midnight and on more than 90 % of days after 3 a.m. until 10 a.m. This is noteworthy because many polar-orbiting, sun-synchronized satellites have an overpass during this period.

3.1.3. Vegetation data

Crop development and internal water content dynamics during the whole season are shown in Fig. 3. The corn leaves reached their maximum size around 25 May when LAI reached its maximum value of 3.8. Results show that variations in the whole-plant gravimetric water content throughout the season (see Fig. S5) are consistent with those reported in Fig. 4 of the study by Togliatti et al. (2019). Before 25 May, the gravimetric water content of both stems and leaves were almost stable. Tassel emergence occurred around 25 May, after which  $M_g$  of both stems and leaves decrease. A sharp decrease is observed after 1 June. Ear formation results in a significant decrease in the  $M_g$  of the stems. The hourly interpolated and the adjusted gravimetric water content of the leaves ( $M_{g+}$ ) calculated using Eq. (7) are also shown in

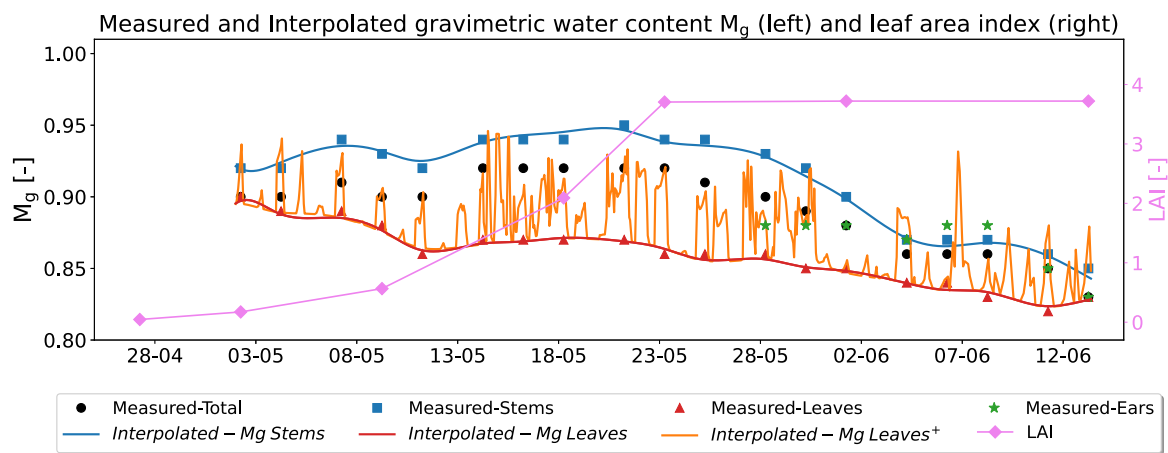


**Fig. 3.** Seasonal pattern of measured LAI and pre-dawn gravimetric water content for total plant and per constituent, in addition to hourly interpolated gravimetric water content of stems and leaves and the adjusted gravimetric water content of corn leaves using the SCW amount ( $M_{g+}$ ). Note that the hourly gravimetric water content values required by the model are calculated by linearly interpolating between the pre-dawn destructive sampling measurements which were obtained three times per week.

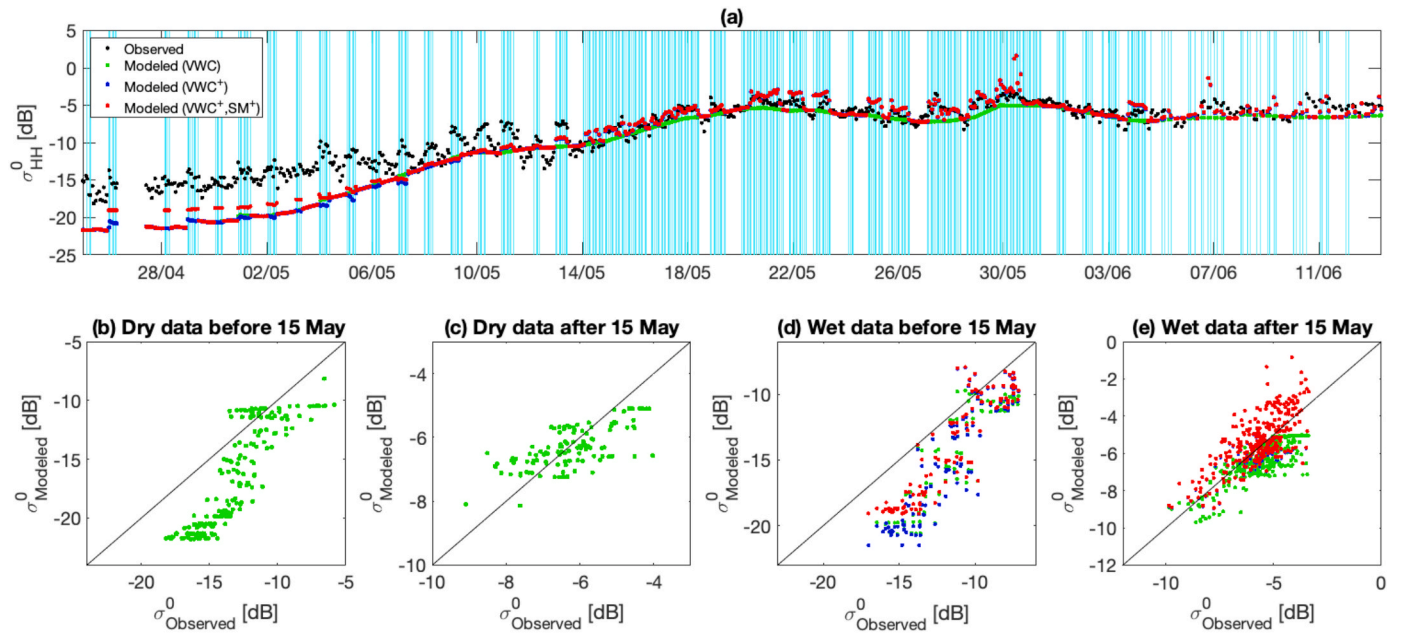


**Fig. 4.** The time series of observed backscatter and modeled backscatter for the three implementations at L-band and HH polarization. Light blue vertical lines indicate the presence of SCW during radar acquisition (a). The scatter plot between the observed and modeled backscatter for data when there was no SCW for time periods before 15 May (bare soil and early season) (b), and after 15 May (mid-to late season) (c). The scatter plot between the observed and modeled backscatter for data when the SCW was presented for time periods before 15 May (bare soil and early season) (d), and after 15 May (mid-to late season) (e). Note that simulations use hourly  $M_g$  values that were obtained by linear interpolation of the pre-dawn destructive measurements obtained three times per week. (For interpretation of the references to color in this figure legend, the reader is referred to the Web version of this article.)

this figure. Note, that the adjusted gravimetric water content never exceeds 1.

### 3.2. Representing the effect of SCW in the Tor Vergata model

Here, we compare the three implementations of the Tor Vergata model in terms of their capacity to simulate total L-band backscatter. The results for these three implementations at L-band for HH, VV, and

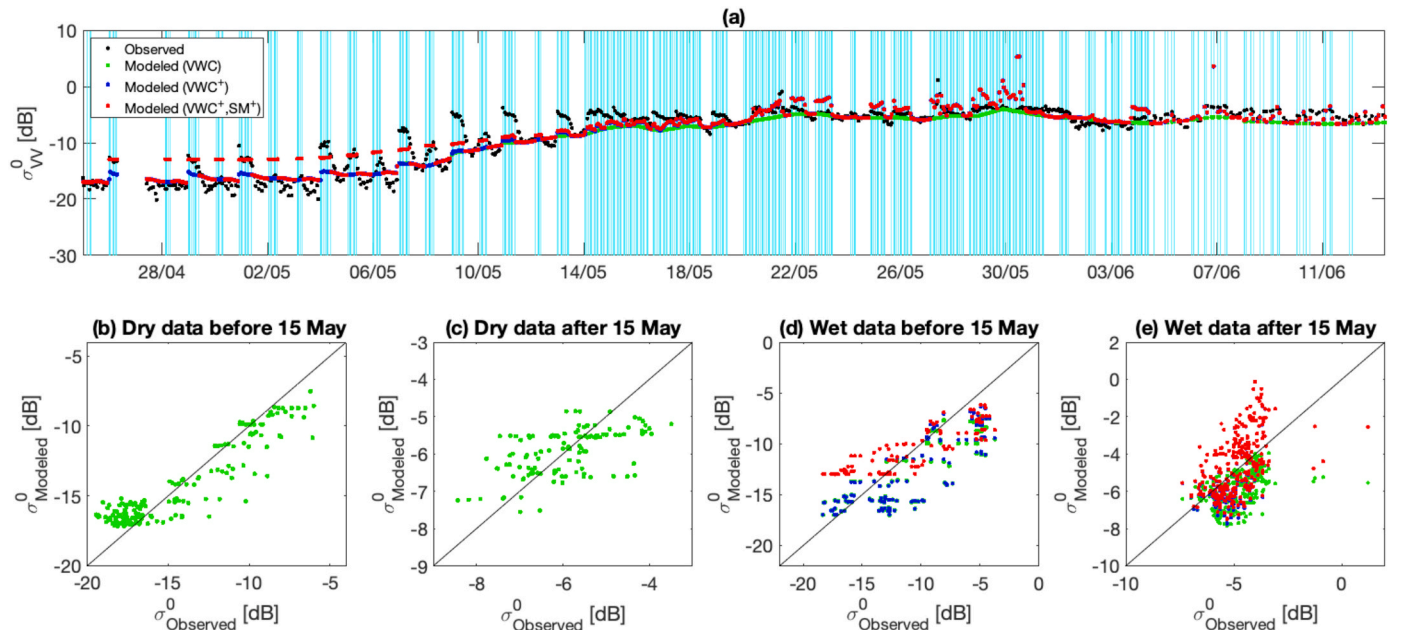


**Fig. 5.** The time series of observed and modeled backscatter for the three implementations at L-band and VV polarization. Light blue vertical lines indicate the presence of SCW during radar acquisition (a). The scatter plot between the observed and modeled backscatter for data when there was no SCW for time periods before 15 May (bare soil and early season) (b), and after 15 May (mid-to late season) (c). The scatter plot between the observed and modeled backscatter for data when the SCW was presented for time periods before 15 May (bare soil and early season) (d), and after 15 May (mid-to late season) (e). Note that simulations use hourly  $M_g$  values that were obtained by linear interpolation of the pre-dawn destructive measurements obtained three times per week. (For interpretation of the references to color in this figure legend, the reader is referred to the Web version of this article.)

XP polarizations are shown in Figs. 4–6 respectively. Statistics describing the agreement between the model and L-band observations are provided in Table 2.

Figs. 4–6(a) show that, in all three implementations, there is poor agreement between simulated and observed L-band backscatter during the bare soil and early vegetative stage (before 15 May). However, the model performance improves during the middle and late season (after 15 May) when the LAI is above 1.5. In Table 2, the RMSE values are always higher for the period before 15 May than the period after 15 May. This is primarily due to the performance of the IEM soil scattering model during the bare soil and early season period. Even for days without SCW, the IEM model does not capture the observed dynamics in radar backscatter due to the change in surface soil moisture. In addition, in HH polarization (Fig. 4), a significant bias occurs due to a challenge related to determining the surface roughness (Álvarez-Mozos et al., 2008), our treatment of which is discussed in Section 2.3, and the presence of system noise in the first few days of this period in HH backscatter (Khabbazan et al., 2021a, 2021b). It worth mentioning that, in the UF-LARS scatterometer, all channels are designed to be independent, which results in independent noise levels. During the first few days of the season, up to May 8th, the power ratios at HH polarization were closer to the noise floor compared to those at VV polarization. This noise led to variability in the backscatter data obtained post-calibration. Despite extensive investigations, the primary reason for this noise remained undetermined and unresolved. These HH data are plotted for completeness but are not used in any quantitative analyses.

In all three polarizations (Figs. 4–6(a)), in the presence of SCW, even when the surface layer is assumed to be fully saturated to represent the presence of SCW, the IEM model underestimates the scattering from the soil surface. In this period, the  $VWC^+$  implementation has a limited effect due to the small size of the corn leaves. However, the  $VWC^+ SM^+$  implementation reduced the RMSE considerably. This will be discussed in detail in Section 3.3.

In the absence of SCW the RMSE and ubRMSE values after 15 May are half of those obtained before 15 May. In addition, the bias is close to zero for data without SCW after 15 May. This can be easily seen by

comparing Figs. 4–6(b) to Figs. 4–6(c). These results show that the standard version of the Tor Vergata model can simulate the observed backscatter from corn in L-band, and in all polarizations (RMSE < 0.85 dB) at the mid and late season (LAI > 1.5) in the absence of SCW.

For data with SCW, the performance of all three Tor Vergata model implementations is better for the period after 15 May (mid to late season) compared with the period before 15 May (early season). This can be seen by comparing Figs. 4–6(d) to Figs. 4–6(e). Comparing the three implementations, the RMSE and bias values after 15 May are always highest for the standard VWC implementation. The reduction in RMSE, and particularly, bias values in the  $VWC^+$  implementation shows that representing the observed SCW as additional internal water content of leaves (Modeled  $VWC^+$ ) leads to some improvement in the agreement between modeled and simulated L-band backscatter. However, the bias is still higher than that observed for data without SCW, suggesting that there is considerable scope for improvement in how SCW on the vegetation can be represented. The additional value of  $VWC^+ SM^+$  over  $VWC^+$  is limited after 15 May due to the limited sensitivity to the soil surface under the fully grown canopy.

### 3.3. The effect of dew on soil

Fig. 7 provides a detailed view of the period before 15 May when the soil is transitioning from bare to light vegetation cover (LAI < 1.5) for VV and XP pol. The HH pol is not included here due to a presence of system noise in the first few days of this period in this channel as explained in section 3.2.

The gradual increase in the observed radar backscatter during this period is related to crop growth (Fig. 3). The daily cycles superimposed on this upward trend are due to dynamics in the soil moisture, internal vegetation water content, and the presence of interception or dew. Midnight irrigation (indicated by the blue background) led to a rapid increase of around  $0.09 \text{ m}^3 \text{ m}^{-3}$  in soil moisture at 5 cm depth which resulted in an increase of more than 5 dB in backscatter in both polarizations. On nights without irrigation, the accumulation of dew from midnight until sunrise (periods indicated by gray background) led to a

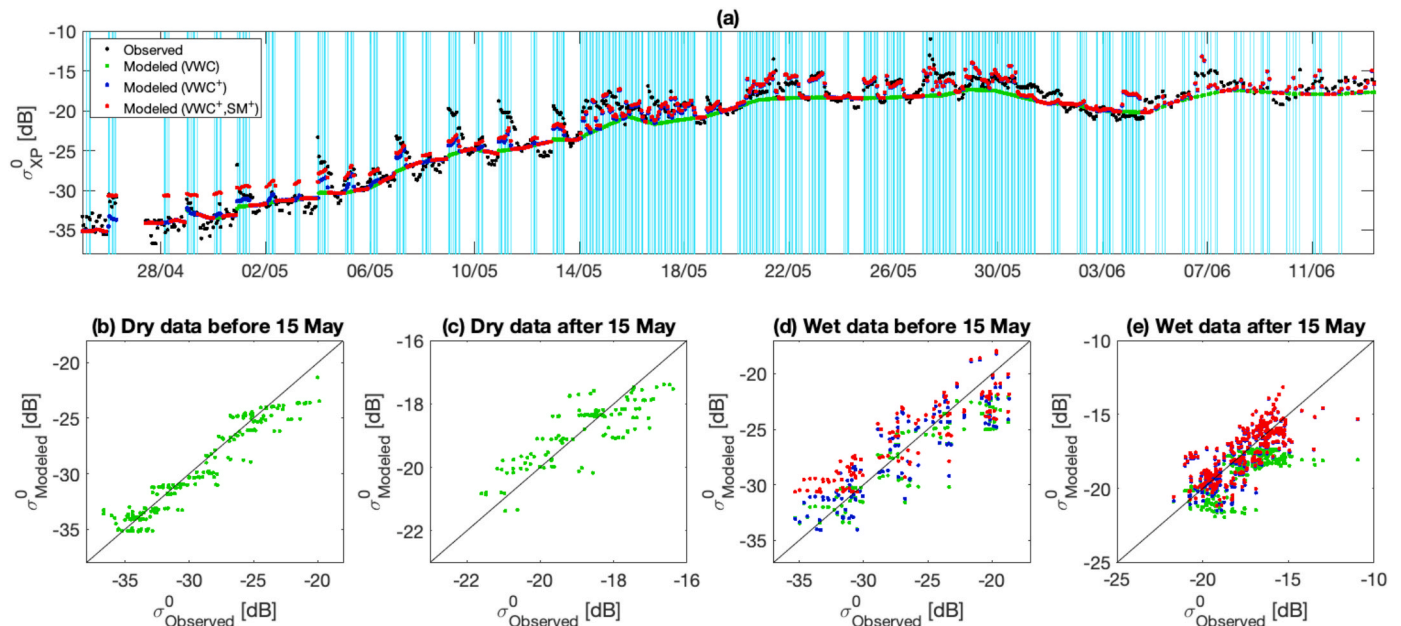


**Fig. 6.** The time series of observed backscatter and modeled backscatter for the three implementations at L-band and cross-polarization (XP). Light blue vertical lines indicate the presence of SCW during radar acquisition (a). The scatter plot between the observed and modeled backscatter for data when there was no SCW for time periods of before 15 May (bare soil and early season) (b), and after 15 May (mid-to late season) (c). The scatter plot between the observed and modeled backscatter for data when the SCW was presented for time periods before 15 May (bare soil and early season) (d), and after 15 May (mid-to late season) (e). Note that simulations use hourly  $M_g$  values that were obtained by linear interpolation of the pre-dawn destructive measurements obtained three times per week. (For interpretation of the references to color in this figure legend, the reader is referred to the Web version of this article.)

**Table 2**

Comparison of modeled and observed backscatter per polarization, where a distinction is made between early (before 15 May) and late (after 15 May) season, as well as between acquisitions obtained in the presence and absence of SCW.

Polarization	Assessment parameter	Model dataset conditions							
		Before 15 May				After 15 May			
		Without SCW		With SCW		Without SCW		With SCW	
		VWC	VWC	VWC+	VWC + SM+	VWC	VWC	VWC+	VWC + SM+
VV	RMSE	1.63	3.18	3.07	2.72	0.85	1.58	1.49	1.46
	UbrMSE	1.62	2.4	2.38	2.71	0.85	1.06	1.49	1.46
	Bias	-0.17	2.09	1.93	-0.18	0.01	1.17	-0.05	-0.09
	R2	0.68	0.55	0.58	0.62	0.79	0.69	0.71	0.72
HH	RMSE	4.24	3.84	3.96	3.06	0.78	1.14	1.05	1.05
	UbrMSE	2.37	1.97	2.27	1.77	0.78	0.79	0.98	0.97
	Bias	3.52	3.3	3.24	2.5	0.08	0.82	-0.37	-0.41
	R2	0.45	0.61	0.62	0.64	0.67	0.68	0.69	0.69
XP	RMSE	1.34	1.84	2.27	2.51	0.73	1.94	1.29	1.25
	UbrMSE	1.26	2.07	2.25	2.38	0.73	1.22	1.28	1.25
	Bias	0.44	1.21	0.33	-0.8	-0.01	1.51	0.13	0.02
	R2	0.39	0.56	0.57	0.59	0.63	0.65	0.66	0.67

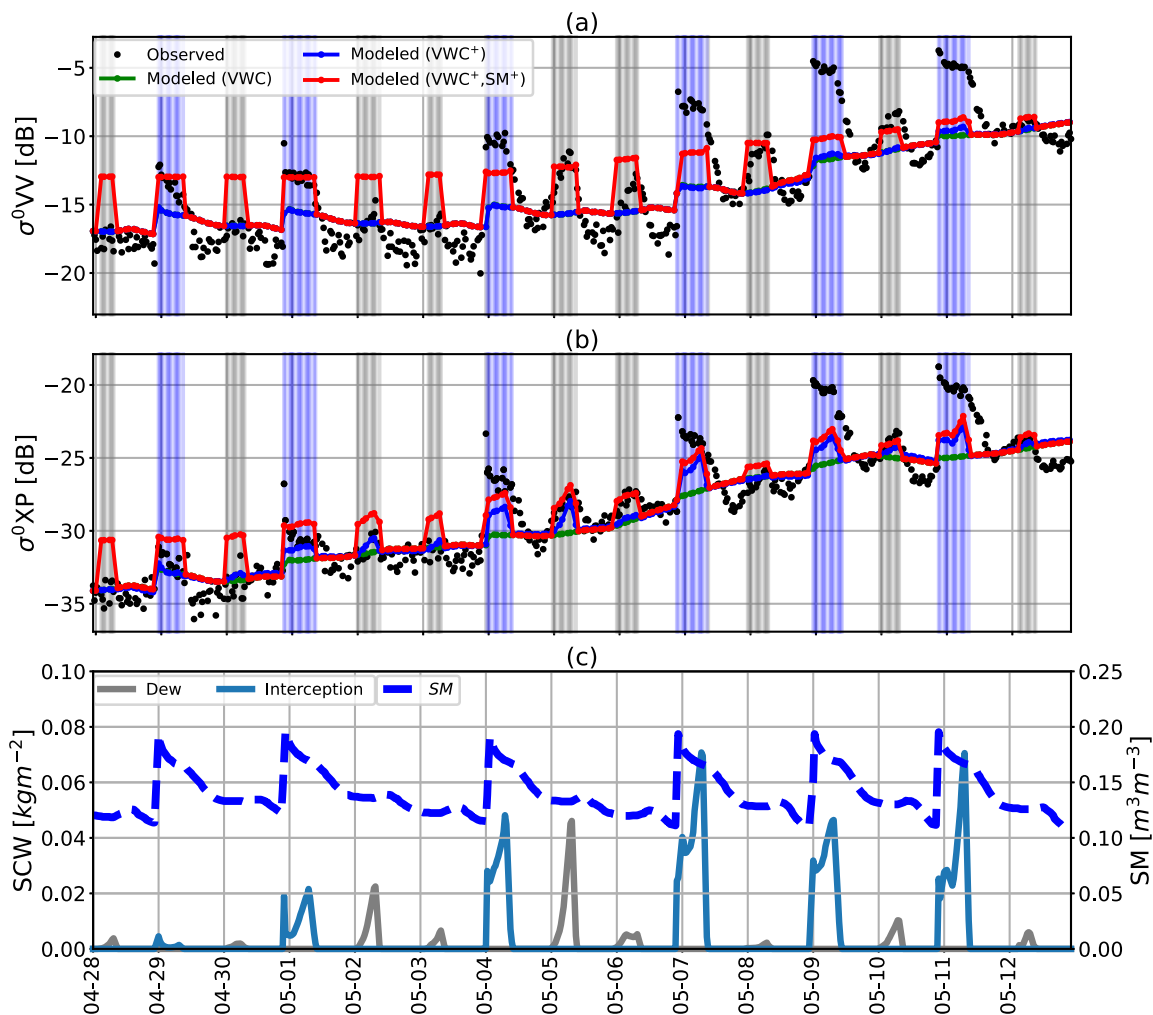


**Fig. 7.** Time series of observed backscatter and modeled backscatter for three implementations in (a) VV-polarization and (b) cross-polarized (XP). The vertical gray and blue lines indicate the presence of dew and interception during the radar acquisition respectively. (c) averaged volumetric soil moisture ( $m^3 m^{-3}$ ) profile at 5 cm, and SCW (dew/interception) amount ( $kg m^{-2}$ ) for 15 days during the early season. Note that simulations use hourly  $M_g$  values that were obtained by linear interpolation of the pre-dawn destructive measurements obtained three times per week. (For interpretation of the references to color in this figure legend, the reader is referred to the Web version of this article.)

gradual increase in backscatter of up to 2–3 dB, even though soil moisture (measured at 5 cm) was steady. Since the corn leaves are small during this period, this increase can be related to the accumulation of dew on the soil surface as discussed by Vermunt et al. (2020); Khabbazan et al. (2021a).

In VV, simulated backscatter from the VWC and VWC<sup>+</sup> implementations are virtually identical. With the exception of 9 and 11 May, the VWC<sup>+</sup> results overlay the VWC results completely. Due to the limited vegetation cover, the total VV backscatter is primarily affected by the soil surface rather than the vegetation. Both implementations simulate the increase in the observed backscatter due to crop growth and biomass accumulation, and the variation in 5 cm soil moisture. But neither captures the observed sub-daily dynamics. The RMSE from the VWC and VWC<sup>+</sup> implementations are 3.18 dB and 3.08 dB in VV. Part of the discrepancy is due to the limitations of the IEM model discussed earlier. However, our working hypothesis is that the failure to account for water on the soil surface explains the lack of sub-daily dynamics. In VV, the VWC<sup>+</sup> SM<sup>+</sup> implementation introduces a steep change in backscatter as soon as any SCW is detected on the leaf wetness sensor. The high values, during the dew and interception period, correspond to the VV backscatter from saturated soil. The value increases from −12 dB on 28 April to −9 dB on 12 May. While this introduces a response in

backscatter at the right time, it is too high for dew events before 4 May, and too low for interception events after 4 May. The VWC<sup>+</sup> SM<sup>+</sup> leads to an increase in ubRMSE compared to VWC<sup>+</sup> because it has limited variability, but it results in a significant reduction in absolute bias.

In cross-pol, the sensitivity of total backscatter to even a small amount of vegetation means that the VWC and VWC<sup>+</sup> simulations can be distinguished during most dew and interception events. The inclusion of additional moisture in the leaves of these young crops is enough to increase backscatter and reduce the bias between simulated and observed XP backscatter. However, even the increase in VWC<sup>+</sup> is not enough to explain the dynamics in backscatter during interception events from 4 May onwards. The effect of VWC<sup>+</sup> SM<sup>+</sup> is most significant in the first few days (before 4 May). Once the XP backscatter starts to increase due to plant growth, the limited difference between VWC<sup>+</sup> and VWC<sup>+</sup> SM<sup>+</sup> suggests that the backscatter is primarily sensitive to the vegetation rather than the soil. Again, it seems that VWC<sup>+</sup> SM<sup>+</sup> is too wet for dew in the first few days but not wet enough to capture interception in the latter half of this period. Table 2 confirms that while there is an increase in the random errors through the inclusion of the extra moisture, there is a considerable reduction in bias in VV and XP using the VWC<sup>+</sup> SM<sup>+</sup> model.

These results illustrate that for low vegetation cover before 15 May

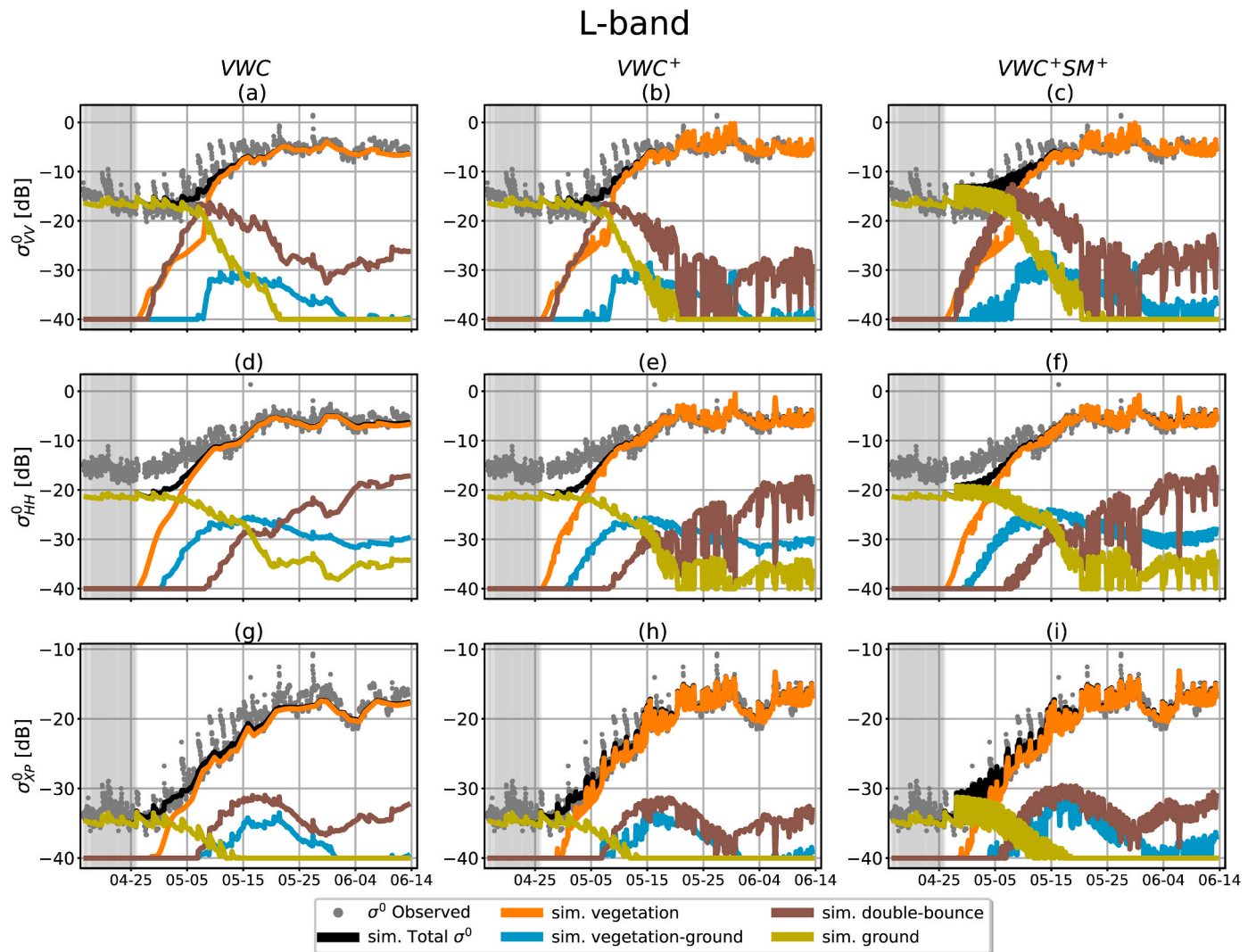


Fig. 8. Tor Vergata model simulations and observed backscatter in L-band for three polarization combinations and three implementations. Each column shows results for one implementation in VV, HH, and XP polarization from top to bottom. The gray background indicates the period when no leaf wetness sensors were installed. Note that simulations use hourly  $M_g$  values that were obtained by linear interpolation of the pre-dawn destructive measurements obtained three times per week.

( $LAI < 1.5$ ), the presence of water on the soil surface during dew and interception events needs to be accounted for. Setting surface soil moisture to saturation in the presence of dew or interception is a pragmatic interim solution, but it provides a conservative estimate of the effect of interception in these conditions. Furthermore, the agreement between model and simulation is still not comparable to the agreement in the absence of SCW. This suggests that there is considerable scope for improvement in how the effect of dew on the soil surface could be represented in the model.

### 3.4. Effect of SCW on scattering mechanisms at L-band

Fig. 8 shows the simulated total backscatter as well as the contributions from each scattering mechanism for the three Tor Vergata model implementations at L-band. The (standard) VWC implementation (Fig. 8 left column) shows that the co-polarized backscatter was dominated by ground scattering until 4 May. From 4 to 15 May, increasing biomass resulted in attenuation of ground scattering and an increase in vegetation scattering, double bounce, and vegetation-ground scattering. After 15 May, when  $LAI > 1.5$ , the simulated backscatter is dominated by vegetation scattering with the double bounce term providing the second largest contribution. During this period, the contributions of ground, and vegetation-ground scattering were negligible in VV-pol (Fig. 8(a)), while in HH-pol (Fig. 8(b)) they had some limited effect. In cross-polarization (Fig. 8(g)), ground scattering was dominant until 29 April. From 29 April (one week after crop emergence) onward, vegetation scattering dominated.

The inclusion of additional internal water in the  $VWC +$  implementation (Fig. 8 middle column), mainly has an effect after 15 May. The presence of SCW led to an increase in the total backscatter in all polarizations mainly due to the increase in the vegetation scattering term. The SCW also slightly increases the vegetation-ground scattering while it reduces the double bounce and ground scattering contributions to close to  $-40$  dB in all polarizations. This illustrates that the presence of SCW affects penetration through the canopy layer, consistent with previous studies (Khabbazan et al., 2021a; Xu et al., 2021).

Accounting for water on the soil surface using the  $VWC + SM +$  implementation during the dew and interception events (Fig. 8 right column) leads to an increase in all contributions except the vegetation scattering term before 15 May. This is mainly due to an increase in ground scattering and vegetation-ground scattering. After 15 May, the combined effect of SCW and dew on the soil surface led to a decrease in double bounce and ground scattering. Comparing the rows in Fig. 8, it is clear that the impact on total backscatter varies somewhat with polarization, depending on the relative importance of the vegetation and ground scattering.

### 3.5. The effect of SCW alone on backscatter

In previous sections, the agreement between observations and simulations of the three implementations at L-band, as well as the contribution of scattering mechanisms was investigated. However, these simulations considered the combined effect of several factors simultaneously: change in internal vegetation water content caused by plant growth, soil moisture, SCW (modeled by adding the amount of SCW as internal water content of corn leaves, denoted as  $M_{g+}$ ), and dew on the soil surface (modeled by considering saturated soil moisture). It is important to clarify that the increase in the internal water content of corn leaves ( $M_{g+}$ ) in our simulations was solely to mimic the impact of SCW. This simulated increase should not be mistaken as an actual change in the internal water content of corn leaves. Moreover, these simulations could not consider the effect of change in observed backscatter due to diurnal changes in water in crop tissue.

Therefore, to understand the influence of SCW alone, we need to compare observations where the only change is in SCW, while the change in soil moisture and internal vegetation water content is

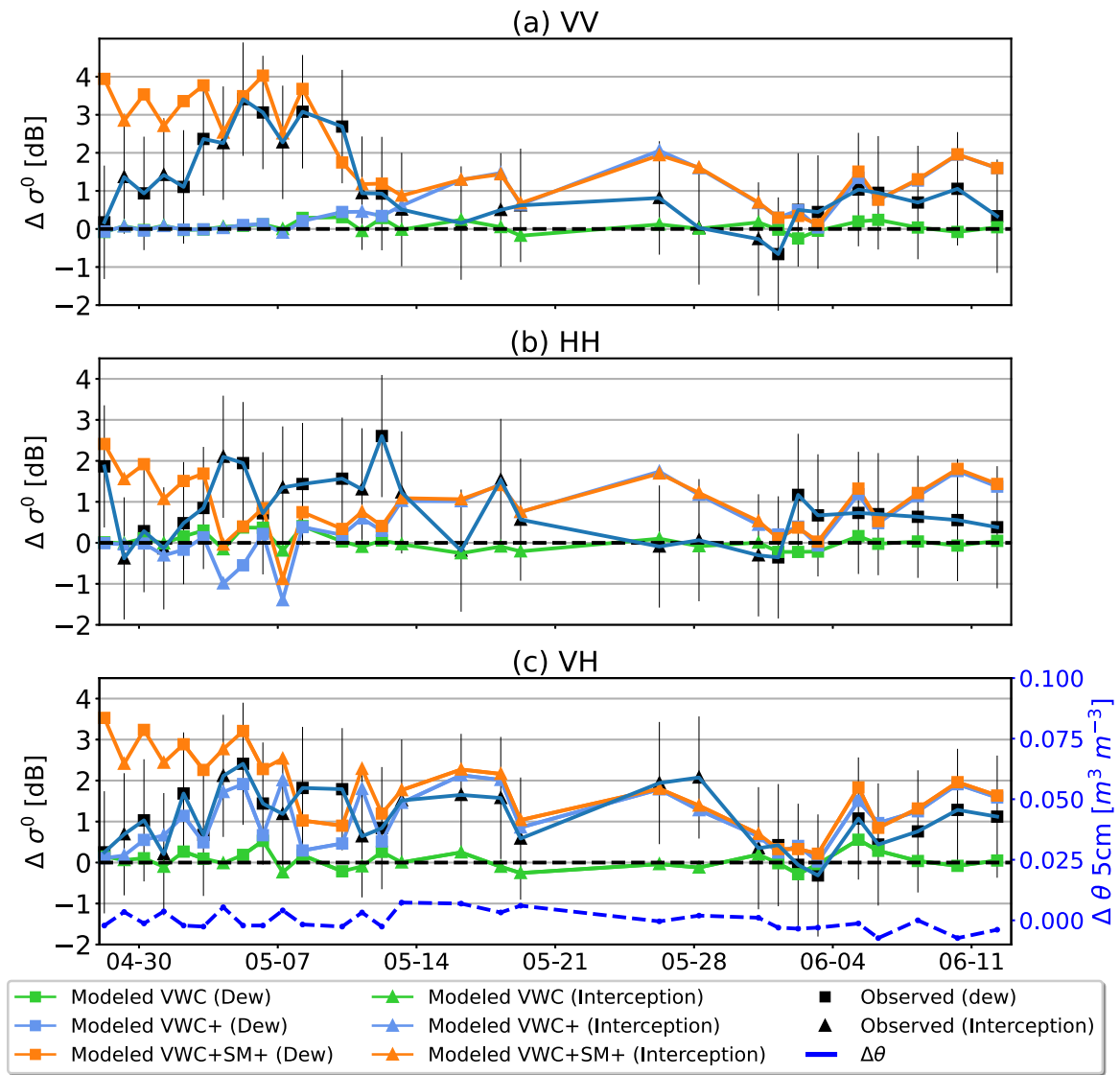
minimal. For this purpose, we will compare backscatter values for times at which we can be sure that the difference is only due to the presence and absence of SCW. Observations at 6 a.m. are used as representative of the presence of SCW, as this time coincides with the maximum SCW amount. It is also pre-sunrise, so the internal water content is at a maximum as discussed by Vermunt et al. (2022a). They found, by estimating transpiration using reference ET and actual sap flow, that the VWC in corn can reach its maximum value around 10 p.m., stay constant until sunrise, and then decrease again after sunrise. To choose data for the absence of SCW or moisture on the soil surface, two times were considered: 10 p.m. on the previous day or 9 or 10 a.m. on the same day.

When morning SCW is due solely to dew, the change in backscatter from 10 p.m. to 6 a.m. of the next day is only related to the accumulation of dew. It is assumed here that crop tissue water does not change during this period based on the finding of Vermunt et al. (2022a). As illustrated in Fig. 9 (c), the coincident difference in soil moisture is less than  $0.007 \text{ m}^3 \text{ m}^{-3}$ . Therefore, its effect on backscatter is considered negligible.

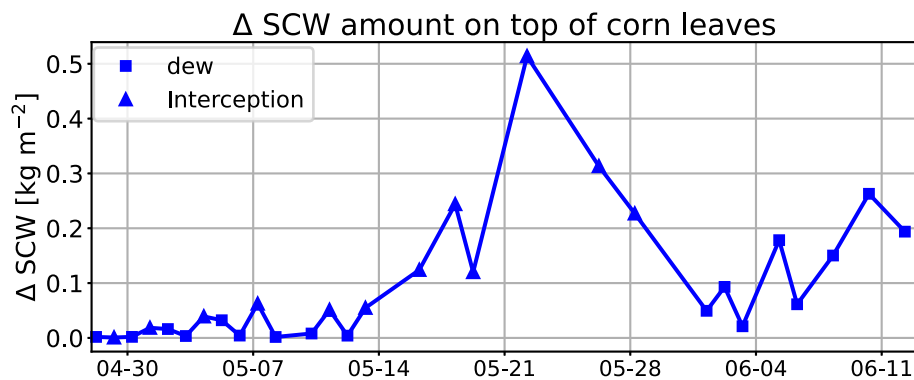
As shown in Fig. S3, irrigation was applied on several dates, generally at night. During these interception events, the 5 cm soil moisture changed considerably between 10 p.m. and 6 a.m., having a significant effect on backscatter between these two times. Therefore, for interception events, the first acquisition after 9 a.m. was used as the observation without SCW to ensure that these are the first acquisitions after the SCW has fully dissipated. The soil moisture data in Fig. 9(c) show that the 5 cm soil moisture variations between 6 a.m. and 9 a.m. are negligible. Therefore the backscatter dynamics in Figs. 9 and 11, and Fig. S4 can mainly be attributed to the presence of water on the vegetation and soil alone. Since VWC may decrease between 6 a.m. and the first acquisition after 9 a.m. (Vermunt et al., 2022a), the  $\Delta\sigma^0$  value due to SCW may be slightly lower than the values reported in these figures. Fig. 10 shows  $\Delta\text{SCW}$  on the corn leaves. For dew events,  $\Delta\text{SCW}$  is defined as the difference between SCW amount at 6 a.m. and 10 p.m. on the previous day. For interception events,  $\Delta\text{SCW}$  is defined as the difference between early morning (6 a.m.) and late morning (after 9 a.m.) SCW. The time series in Fig. 10 shows only days when the leaf wetness sensors indicated no SCW at either 10 p.m. or 9 AM.

Fig. 9 shows  $\Delta\sigma^0$ , the difference between backscatter acquired during the presence and absence of SCW or moisture on the soil surface. Extracting the  $\Delta\sigma^0$  allows us to focus on the ability of the model to capture the  $\Delta\sigma^0$  rather than the absolute value of  $\sigma^0$ . Fig. 9 shows that variations in  $\Delta\sigma^0$  during the season is in average around 1.18 dB for co-pol and 1.2 dB for cross-pol, and can reach up to 3.41, 2.60 and 2.41 dB in VV, HH and XP polarizations respectively. Fig. 9 shows that the  $\Delta\sigma^0$  values from the standard (VWC) model implementation are close to zero and that this implementation does not capture the observed  $\Delta\sigma^0$  values in L-band. For the period before 15 May, the  $VWC +$  implementation does not capture the  $\Delta\sigma^0$  values in the observed VV or HH backscatter (Fig. 9(a) and (b)). In VV, the  $VWC +$  implementation is indistinguishable from the VWC implementation due to the lack of sensitivity to vegetation in the bare soil and early vegetative stages. This could be related to the fact that considering only the water on the leaves mostly affects the direct vegetation term which is small at this time. Allowing for wet stems may lead to an increase vegetation-ground interaction.  $VWC +$  introduces some dynamics in  $\Delta\sigma^0$  in HH, but it does not improve the estimation. Recall, however, that the characterization of roughness in IEM in HH-polarization resulted in poor simulations during this time. In XP, the  $VWC +$  implementation improves the simulated  $\Delta\sigma^0$ .

Recall from Fig. 7 (a) that for the period before 15 May, the dynamic range of the model for  $VWC + SM +$  implementation was limited resulting in a maximum  $\sigma^0$  value (red data) higher than that observed during dew events but lower than observed during interception. However, in Fig. 9 (a) the  $\Delta\sigma^0$  estimated for  $VWC + SM +$  implementation during interception events (May 4 to May 15) from the models agrees well with the observed  $\Delta\sigma^0$  with RMSE of 0.28 dB and bias of  $-0.27$  dB. Moreover, the  $VWC + SM +$  implementation produces a larger



**Fig. 9.** Time series of difference in early morning observed and modeled L-band backscatter ( $\Delta\sigma^0$ ) for three implementations from vegetation with and without SCW in (a) VV polarization, (b) HH polarization, and (c) cross-polarization (XP). The difference is calculated between 6 a.m. and 10 p.m. of a day before for dew events and between 6 a.m. and late morning (after 9 a.m.) for interception events. For reference, the error bars indicate the overall uncertainty (1.49 dB) of the UF LARS. The difference in 5 cm soil moisture values for the canopy with and without SCW is shown in (c). Note that simulations use hourly  $M_g$  values that were obtained by linear interpolation of the pre-dawn destructive measurements obtained three times per week.



**Fig. 10.** Time series of difference in surface canopy water amount  $\text{kg m}^{-2}$  on top of corn leaves between 6 a.m. and 10 p.m. of a day before for dew events and between 6 a.m. and late morning (after 9 a.m.) for interception events. The  $\Delta\text{SCW}$  was calculated only for days when the leaf wetness sensors indicated no SCW at either 10 p.m. or 9 AM.

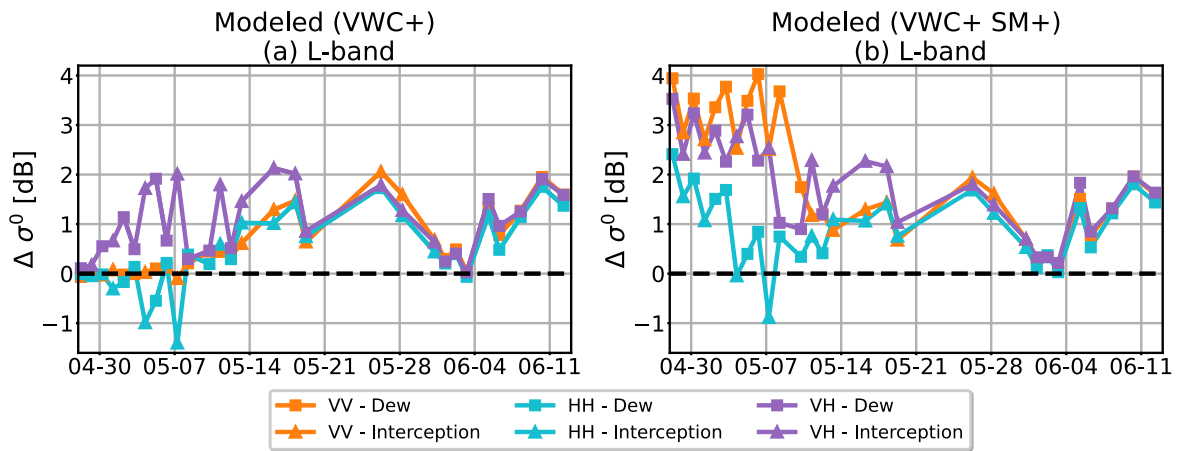


**Fig. 11.** Time series of the difference in early morning simulated total backscatter ( $\Delta\sigma^0$ ) from vegetation with and without SCW, for three polarizations at L-band. The  $VWC^+$  implementation is shown in the left column and for  $VWC^+ SM^+$  implementation is shown in the right column. Note that simulations use hourly  $M_g$  values that were obtained by linear interpolation of the pre-dawn destructive measurements obtained three times per week.

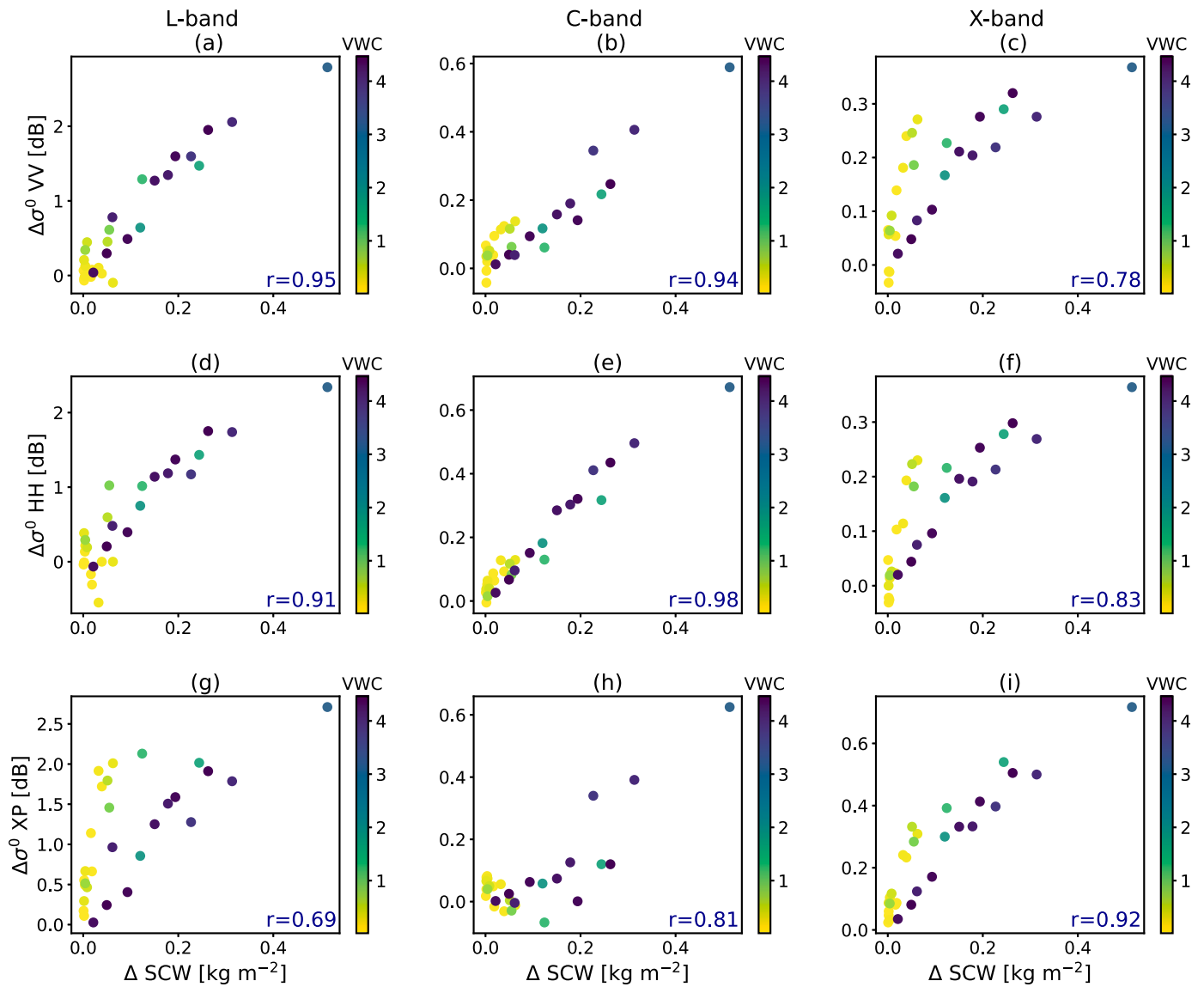


**Fig. 12.** The relationship between  $\Delta\sigma^0$  ( $VWC^+$  implementation) and the  $\Delta SCW$  for three polarizations and L-, C-, X-band is shown. The color for each data point shows the amount of VWC for the 6 a.m. acquisition. Pearson correlation coefficients are shown in the bottom right of each plot. (For interpretation of the references to color in this figure legend, the reader is referred to the Web version of this article.)

$\Delta\sigma^0$  during dew events (squares) compared to interception events (triangles) for this period, while the observed data shows that the  $\Delta\sigma^0$  from interception is not always lower than those of the dew. This can be related to the fact that the dew on the soil surface does not penetrate to 5 cm depth. Therefore assuming the saturated soil moisture at 5 cm depth to model the effect of dew on the soil surface can cause an overestimation of the isolated effect of dew compared to interception, which can be an indication that dew on the soil surface is not represented in an optimal way. In XP, Fig. 9 (c) shows that the  $VWC^+$  implementation could model the  $\Delta\sigma^0$  from SCW and moisture on the soil surface before 15 May better than  $VWC^+ SM^+$  implementation, while results in Fig. 7 showed the  $VWC^+ SM^+$  implementation better captured the absolute values of the  $\sigma^0$  than  $VWC^+$  implementation.

For the period after 15 May, sensitivity to the soil surface is limited and the total backscatter is dominated by the vegetation scattering (Fig. 8), so the  $\Delta\sigma^0$  estimated using the  $VWC^+$  and  $VWC^+ SM^+$  implementations are virtually identical. Between 15 May and 1 June, the  $\Delta\sigma^0$  from both implementations is higher than observed. Recalling Figs. 6–8, this is during the high biomass period ( $LAI > 1.5$ ) which was also very wet. The observed  $\sigma^0$  was close to saturation, however, the model  $VWC^+$  and  $VWC^+ SM^+$  could still increase in the presence of SCW. After 1 June, results show that both implementations simulate the observed  $\Delta\sigma^0$  with higher accuracy except for the last two dates. The overestimation on these two dates could be related to the fact that the corn reached its maximum biomass after 25 May and the amount of SCW was very high on those dates (Fig. 10).

Fig. 11 shows simulated  $\Delta\sigma^0$  at L-band using the  $VWC^+$  and the  $VWC^+ SM^+$  implementations. Similar simulated results for C- and X-band is shown in Fig. S4 in the supplementary material. Comparing the results in Fig. 11 and Fig. S4 left column, it is clear that the magnitude of the difference due to water on the canopy may vary by frequency. The modeled  $\Delta\sigma^0$  can reach up to around 2.5 dB in L-band, while simulation in C- and X-band suggest lower value of around 0.6 dB. It should be noted that although the simulations in Fig. 9 could not capture  $\Delta\sigma^0$  dynamics perfectly, the simulations approximate the maximum and average magnitude of the change in  $\Delta\sigma^0$  during the season. Based on the simulation results in Fig. S4, during the interception events in the middle of the season, the simulated  $\Delta\sigma^0$  values at C-band in various polarizations are comparable in magnitude. In X-band, the  $\Delta\sigma^0$  in XP is larger than that in co-polarized backscatter. Results also suggest that the effect of water on the vegetation is lower during the early season (especially in co-polarized channels) and reaches its maximum during the mid and high season as crop reaches its maximum biomass.

Fig. 12 shows the relationship between  $\Delta SCW$  and the modeled  $\Delta\sigma^0$  in L-, C-, and X-band from the  $VWC^+$  implementation. The Pearson correlation coefficients are relatively high for all frequencies and polarizations. Fig. 12 highlights the contrast between frequencies in terms of sensitivity, and shows that the relationship between  $\Delta SCW$  and  $\Delta\sigma^0$  evolves with VWC as the contribution of direct scattering to total backscatter changes. The highest amount of SCW on 22 May ( $0.52 \text{ kg m}^{-2}$ ), caused by the heaviest rain event during the growing season (Fig. S3 in supplementary material), resulted in a peak on  $\Delta\sigma^0$  at L-, C-, and X-band (Fig. 11 and Fig. S4 left column). The reduction in the amount of  $\Delta SCW$  from 22 May until 4 June resulted in the reduction in modeled  $\Delta\sigma^0$  in all polarization at 3 bands. The rapid increase in  $\Delta SCW$  between 6 and 11 June happened due to the heavy rain event on 7 June and heavy dew event on 10 June. It should be noted that based on the L-band data from Fig. 9, the  $\Delta\sigma^0$  in this period could also overestimate the effect of dew on C- and X-band. In X-band, the effect of SCW was highest in XP polarization which can be explained by the scattering mechanisms. However, in this study due to the lack of experimental evidence on higher frequencies, the scattering mechanism was not investigated.

Fig. 11 (b) shows that in L-band, the effect of water on the soil surface at the early season can be as significant as the effect of water on the vegetation later in the season and both cases can affect the signal around 2.5–3.5 dB. However, in C- and X-band (Figs. S4(b) and (d)), simulation

results suggest that accounting for the effect of dew on the soil surface during the bare soil and early vegetative stage could have a stronger effect than the presence of SCW during the mid and late season. Simulation results also suggest that dew on the soil surface during the bare soil and early season could affect the radar signal in C- and X-band for up to 3 dB, while the effect of SCW during the mid and late season can only affect the simulated signal for up to 0.6 dB. However, due to a lack of experimental evidence on these frequencies, further investigation is required to be able to make a firm conclusion.

The simulation results presented in Fig. S4 suggest that the water on the canopy could have a limited impact in C- and X-band but that water on the soil surface at the beginning of the season could have a comparatively large effect. Results in Fig. 11(b) and Figs. S4(b) and (d) also suggest that the effect of dew on the soil surface mostly decreases with the increase in crop biomass. The reduction in the sensitivity of backscatter to water on the soil surface diminishes earlier at higher frequencies. This finding is very relevant for applications such as soil moisture estimation over bare soil or sparsely-vegetated areas when the combined data from ascending and descending overpasses would be used at C- and X-band. If data from ascending and descending overpasses are combined without considering the effect of the presence of dew on the soil surface, it could lead to spurious soil moisture values.

#### 4. Discussion

This study provides new insights into the effect of SCW on radar backscatter and various contribution to total backscatter. The observations and model simulations suggest that the presence of dew and interception can reach up to 2.5 dB at L-band. To put these variations in context, note that while the overall uncertainty of the ground-based UFLARS was approximately 1.49 dB (Liu et al., 2016), the maximum impact of changes in soil moisture and the dynamic range in backscatter due to crop growth at L-band was around 5 dB and 10 dB, respectively. The presence of dew and/or intercepted precipitation can lead to a change corresponding to 25%–50% of the expected dynamic range in this vegetation type. Therefore, both observations and model simulations suggest that the presence of dew and intercepted precipitation should be considered at low microwave frequencies. This is relevant for current SAR missions such as SAOCOM, and ALOS as well as upcoming SAR missions, like NISAR and ROSE-L. In addition, this sensitivity of sub-daily SAR data to water on the canopy suggests that future sub-daily SAR data could be valuable in understanding the influence of interception on evaporation and evaporation partitioning. This is relevant in the context of Cosmo SkyMed, TerraSAR-X and TanDEM-X and data from commercial constellations such as those from Capella Space and ICEYE.

Simulations results in Fig. 11 and Fig. S4 suggest that the isolated effect of dew on the soil surface during the early season on backscatter could reach up to 3.8 dB in all bands. These simulation results suggest that while the presence of SCW potentially illustrated limited impact at higher frequencies, the presence of dew on the soil surface at the beginning of the season should be considered during bare soil and low vegetation cover for all frequencies. To our knowledge, this is the first study to consider the influence of dew on soil on backscatter. Measuring this quantity directly is challenging because, while some soil moisture sensors like Hydra Probes have large measurement volumes of around  $30\text{--}40 \text{ cm}^3$ , most sensors designed for more localized soil moisture measurements such as EM-5 sensors need to be buried beneath the surface and typically measure a volume extending a few centimeters around the sensor. While we assumed the leaf wetness sensors could detect the events, additional research is recommended to explore the potential to observe this more deliberately during field experiments using commercial-off-the-shelf (COTS) sensors and providing a more direct method to quantify the amount of water on the soil surface.

Our exploration of C- and X-band is limited to model simulations due to the lack of observational data at these frequencies. Recall from

Section 2.3 that the Tor Vergata model has been validated extensively at C- and X-band as well as L-band. The use of the UF LARS L-band data demonstrates the value and importance of tower-based radar experiments to improve our understanding of microwave interactions with vegetation and to guide model development to support future applications and exploitation of future satellite missions. Our simulated results provide valuable insights, but higher frequency observational data are essential to make these findings definitive. In addition, this study highlights the need to develop realistic representations of dew and interception on the vegetation and soil surfaces in EM models. With the number of radar satellites, and novel applications of their data on the rise, these model developments are urgently needed to enable the use of SAR to model rapid water processes in the soil-vegetation-atmosphere continuum.

Finally, the impact of SCW extends beyond radar backscatter, influencing parameters like differential interferometry, phase differences, polarimetry, and interferometric coherence. Studies such as the TROPISCAT Experiment over tropical dense forests (Essebetey et al., 2019, 2021; Minh et al., 2014; Hamadi et al., 2017), and studies using the BorealScat on boreal forest areas (Monteith and Ulander, 2021a, 2021b; Ulander et al., 2018) have explored the effect of SCW on interferometric coherence, particularly how rain and wind cause temporal decorrelation in tropical and boreal forests. Yet, the impact of dew accumulation, especially heavy dew, on interferometric coherence in temperate agricultural regions remains unclear. A study conducted by Brancato et al. (2017) investigated the relationship between plant surface moisture and differential interferometric observables, such as the magnitude and phase of the interferometric coherence, in a controlled electromagnetic experiment. This study highlighted potential misinterpretations of moisture changes on top of the canopy either for soil water content or fresh biomass variations. Future research should further investigate SCW effects using polarimetry, interferometry and backscatter across a range of cover types.

## 5. Conclusions

The goal of this study was to improve our understanding of the influence of surface canopy water (SCW) on radar backscatter as a function of frequency and polarization. Observations were available from the UF LARS tower-based radar at L-band. In a previous study, these data had been analyzed against continuous leaf wetness sensor, soil moisture and crop geometry data to quantify the impact of SCW on observed L-band backscatter. Here, the L-band observations were compared to three implementations of the Tor Vergata model in which we attempted to account for the presence of SCW by increasing the vegetation and soil moisture contents. These L-band simulations provide insight into the contributions to total backscatter and how they may be affected by the presence of SCW.

The standard implementation of the Tor Vergata model accounts for internal vegetation water content, but does not explicitly consider the presence of SCW. One approach to account for the additional water present due to dew or interception would be to allow for a "cloud" of water droplets throughout the vegetation layer or specifically the leaf layer. However, SCW within the vegetation layer due to dew or interception is primarily concentrated on the leaves and so the additional water should be located at the leaves. Therefore, we accounted for the additional water present of SCW on the vegetation by augmenting the VWC, so that the additional water present as dew or interception is spatially distributed within the dielectric medium according to the geometry and architecture of the vegetation. In other words, the structural representation of the scatterers is the same, but they are wetter. Results at L-band from Table 2, showed that the  $VWC^+$  implementation improved the agreement between simulated and observed backscatter particularly when total backscatter was dominated by the impact of vegetation. This can be seen from the reduction of 0.09 dB, 0.09 dB, and 0.65 dB in the RMSE and the reduction of 1.12 dB, 0.45 dB and 1.38 dB

in the bias for VV, HH, XP respectively. However, while the bias was considerably reduced from 1.17 dB, 0.82 dB, and 1.51 dB–0.05 dB, –0.37 dB, and 0.82 dB in VV, HH, and XP respectively, the agreement between model simulations and observations was far from perfect. Further improvements are necessary and could include, for example, the addition of a thin layer of droplets on the surface of the leaves. This would ensure that the spatial distribution was consistent with that of the vegetation elements, while representing the additional water as "free" water on the leaf surface.

Agreement between the  $VWC^+$  simulations and the L-band observations was comparatively poor during the bare soil and early vegetative stages. We hypothesized that this could be due to the presence of dew, in the form of water on top of the soil layer. We investigated if the effect on backscatter could be emulated by assuming the surface soil layer was saturated if the leaf wetness sensor indicated the presence of moisture on the field. This improved the agreement between the modeled and observed backscatter during the bare soil and early vegetative stages somewhat. However, the remaining mismatch suggests that this approach is less than optimal and should be improved. In past studies, the inclusion of a litter layer has proved beneficial in the simulation of emission and scattering from forest areas (Della Vecchia et al., 2007b; Dente et al., 2014). So, one option could be to represent dew as a thin saturated litter layer. Alternatively, it may be physically more plausible to include an additional thin layer of water droplets on the surface above the soil when the leaf wetness sensors indicate the presence of moisture. Nonetheless, the comparison of simulated and observed L-band backscatter suggests that while there is room for improvement, the  $VWC^+$   $SM^+$  implementation provides better agreement with observations than the standard (VWC) or  $VWC^+$  implementations. This can be seen by reduction of 0.46 dB (VV) and 0.78 dB (HH) in the RMSE and a reduction in bias from 2.09 dB, 3.3 dB and 1.21 dB to –0.18 dB, 2.5 dB and –0.8 dB in VV, HH, XP respectively. It provides some insight into the importance of water on the soil surface during the bare and early growing stages.

Analysis of the contributions of the various scattering mechanisms at L-band shows that including the SCW as additional internal water content of leaves, in general, led to an increase in vegetation volume contribution and a reduction in the contribution from double bounce and direct scattering from the ground in all bands. This finding is consistent with Riedel et al. (2002) and Riedel and Schmulius (2003a, b), who also observed an increase in volume scattering and a decrease in surface and double-bounce scattering based on use of the target decomposition theorem at L-band in the presence of SCW. Assuming a saturated surface soil layer to model the effect of dew on the soil surface has a significant effect on the scattering mechanisms during the bare soil and early season. This generally led to an increase in all contributions except the vegetation volume contribution. The influence of surface soil moisture or water at the soil surface is less important when the vegetation starts to dominate the total backscatter. Therefore, accounting for water on the soil surface is primarily important during the bare soil and early vegetative stages. While Wood et al. (2002) also found that the presence of dew increases radar backscatter during dawn acquisitions, our study is the first to highlight the importance of considering the presence of dew on the soil surface at the beginning of the season potentially for all frequencies, particularly for applications involving bare soil and low vegetation cover.

The Tor Vergata model was also used to explore the potential sensitivity of backscatter to SCW as a function of frequency and polarizations. Simulated results of  $\Delta\sigma^0$  due solely to SCW on backscatter were always low during the early season and reached a maximum during the mid and late season. This effect varied with polarization and frequencies, with simulations suggesting that the impact of SCW alone on backscatter could reach up to 2.5 dB in L-band and likely less at higher frequencies. This finding emphasizes the importance of considering SCW in low frequency data, in agreement with the findings of Wood et al. (2002). This is in contrast to the findings of Gillespie et al. (1990), who

observed a higher increase in radar backscatter at C-band than at L-band during dew events. However, the different conclusions may be due to the difference in crop type (wheat versus corn). Additionally, our findings differ from those reported by Riedel et al. (2002) and Riedel and Schmulius (2003a,b), who observed no significant influence from dew events on VV-pol at L-band. While they studied a similar crop type as this study (corn), the different conclusions may be related to their comparatively sparse dataset (using data from 2 days to 3 times of the day: 6 a.m., 9 a.m., and 12 p.m.). They also used indirect measures, such as microclimatological data, to infer the presence of SCW. In contrast, our study could avail of high temporal resolution radar data combined with direct, continuous measurements of the SCW amount from leaf wetness sensors throughout the entire growing season. The divergence among previous studies underscores the complexities inherent in understanding the impact of SCW on radar observables. While our simulated results provide valuable insights, but higher frequency observational data are essential to make these findings definitive. In addition, further ground-based studies and modeling experiments are recommended to extend the finding of this study to a wider range of land cover types and frequencies.

### CRedit authorship contribution statement

**S. Khabbazan:** Writing – review & editing, Writing – original draft, Methodology, Formal analysis, Data curation, Conceptualization. **S.C. Steele-Dunne:** Writing – review & editing, Supervision, Resources, Project administration, Methodology, Investigation, Funding acquisition, Data curation, Conceptualization. **P.C. Vermunt:** Writing – review & editing, Data curation. **L. Guerriero:** Writing – review & editing, Validation, Resources, Methodology, Conceptualization. **J. Judge:** Writing – review & editing, Resources, Data curation.

### Declaration of competing interest

The authors declare that they have no known competing financial interests or personal relationships that could have appeared to influence the work reported in this paper.

### Data availability

Data will be made available on request.

### Acknowledgment

This project was supported by Vidi Grant 14126 from the Dutch Technology Foundation STW, which is part of The Netherlands Organisation for Scientific Research (NWO), and which is partly funded by the Ministry of Economic Affairs.

### Appendix A. Supplementary data

Supplementary data to this article can be found online at <https://doi.org/10.1016/j.srs.2024.100137>.

### References

- Acuña, M., Ferrazzoli, P., Guerriero, L., 2019. Modeling L-and X-band backscattering of wheat and tests over fields of pampas. *Eur. J. Rem. Sens.* 52, 84–101.
- Agam, N., Berliner, P.R., 2006. Dew formation and water vapor adsorption in semi-arid environments — a review. *J. Arid Environ.* 65, 572–590.
- Allen, C.T., Ulaby, F.T., 1984. Modeling the backscattering and transmission properties of vegetation canopies. Contractor Rep.(CR). Report/Patent Number: NAS 1.26: 171864, NASA-CR-171864, Accession Number: 85N27320.
- Álvarez-Mozos, J., González-Audicana, M., Casali, J., Larranaga, A., 2008. Effective versus measured correlation length for radar-based surface soil moisture retrieval. *Int. J. Rem. Sens.* 29, 5397–5408.
- Baghdadi, N., Gherboudj, I., Zribi, M., Sahebi, M., King, C., Bonn, F., 2004. Semi-empirical calibration of the IEM backscattering model using radar images and moisture and roughness field measurements. *Int. J. Rem. Sens.* 25, 3593–3623.
- Baghdadi, N., Holah, N., Zribi, M., 2006. Calibration of the integral equation model for SAR data in C-band and HH and VV polarizations. *Int. J. Rem. Sens.* 27, 805–816.
- Blaes, X., Defourny, P., Wegmuller, U., Della Vecchia, A., Guerriero, L., Ferrazzoli, P., 2006. C-band polarimetric indexes for maize monitoring based on a validated radiative transfer model. *IEEE Trans. Geosci. Rem. Sens.* 44, 791–800.
- Bracaglia, M., Ferrazzoli, P., Guerriero, L., 1995. A fully polarimetric multiple scattering model for crops. *Rem. Sens. Environ.* 54, 170–179.
- Brancato, V., Liebisch, F., Hajnsek, I., 2017. Impact of plant surface moisture on differential interferometric observables: a controlled electromagnetic experiment. *IEEE Trans. Geosci. Rem. Sens.* 55, 3949–3964.
- Cobos, D.R., 2013. Predicting the Amount of Water on the Surface of the LWS Dielectric Leaf Wetness Sensor. Decagon Devices, Inc. Pullman, WA, USA, Appl. Note, 14556–01.
- Dawson, T.E., Goldsmith, G.R., 2018. The value of wet leaves. *New Phytol.* 219, 1156–1169.
- De Jeu, R.A., Heusinkveld, B.G., Vugts, H., Holmes, T.R., Owe, M., 2004. Remote sensing techniques to measure dew: the detection of canopy water with an L-band passive microwave radiometer and a spectral reflectance sensor. In: *Remote Sensing for Agriculture, Ecosystems, and Hydrology VI*, SPIE, pp. 225–235.
- Della Vecchia, A., Bruni, L., Ferrazzoli, P., Guerriero, L., 2004. Recent advances in crop modeling: the curved leaf and the hollow stem. In: *2004 IEEE International Geoscience and Remote Sensing Symposium (IGARSS)*, pp. 895–898. IEEE.
- Della Vecchia, A., Ferrazzoli, P., Guerriero, L., Blaes, X., Defourny, P., Dente, L., Mattia, F., Satalino, G., Strozzi, T., Wegmuller, U., 2006a. Influence of geometrical factors on crop backscattering at C-band. *IEEE Trans. Geosci. Rem. Sens.* 44, 778–790.
- Della Vecchia, A., Ferrazzoli, P., Guerriero, L., Ninivaggi, L., Strozzi, T., Wegmuller, U., 2008. Observing and modeling multifrequency scattering of maize during the whole growth cycle. *IEEE Trans. Geosci. Rem. Sens.* 46, 3709–3718.
- Della Vecchia, A., Ferrazzoli, P., Guerriero, L., Strozzi, T., Wegmuller, U., 2007a. A statistical and theoretical study about radar sensitivity to crop growth from S to X band. In: *2007 IEEE International Geoscience and Remote Sensing Symposium*, pp. 1424–1427. IEEE.
- Della Vecchia, A., Ferrazzoli, P., Wigneron, J.P., Grant, J.P., 2007b. Modeling forest emissivity at L-band and a comparison with multitemporal measurements. *Geosci. Rem. Sens. Lett. IEEE* 4, 508–512.
- Della Vecchia, A., Guerriero, L., Bruni, L., Ferrazzoli, P., 2006b. Hollow cylinder microwave model for stems. *J. Electromagn. Waves Appl.* 20, 301–318.
- Dente, L., Ferrazzoli, P., Su, Z., Van Der Velde, R., Guerriero, L., 2014. Combined use of active and passive microwave satellite data to constrain a discrete scattering model. *Rem. Sens. Environ.* 155, 222–238.
- Eom, H.J., Fung, A., 1984. A scatter model for vegetation up to Ku-band. *Rem. Sens. Environ.* 15, 185–200.
- Essebey, S.E.I., Villard, L., Borderies, P., Koleck, T., Burbán, B., Le Toan, T., 2021. Long-term trends of P-Band temporal decorrelation over a tropical dense forest—experimental results for the BIOMASS mission. *IEEE Trans. Geosci. Rem. Sens.* 60, 1–15.
- Essebey, S.E.I., Villard, L., Borderies, P., Koleck, T., Monvoisin, J.P., Burbán, B., Le Toan, T., 2019. Temporal decorrelation of tropical dense forest at C-band: first insights from the TropiScat-2 experiment. *Geosci. Rem. Sens. Lett. IEEE* 17, 928–932.
- Ferrazzoli, P., Guerriero, L., 1995. Radar sensitivity to tree geometry and woody volume: a model analysis. *IEEE Trans. Geosci. Rem. Sens.* 33, 360–371.
- Ferrazzoli, P., Guerriero, L., 1996. Emissivity of vegetation: Theory and computational aspects. *J. Electromagn. Waves Appl.* 10, 609–628.
- Ferrazzoli, P., Guerriero, L., Quesney, A., Taconet, O., Wigneron, J.P., 1999a. Investigating the capability of C-band radar to monitor wheat characteristics. In: *IEEE 1999 International Geoscience and Remote Sensing Symposium (IGARSS)*, pp. 723–725. IEEE.
- Ferrazzoli, P., Guerriero, L., Schiavon, G., 1999b. Experimental and model investigation on radar classification capability. *IEEE Trans. Geosci. Rem. Sens.* 37, 960–968.
- Fung, A.K., Li, Z., Chen, K.S., 1992. Backscattering from a randomly rough dielectric surface. *IEEE Trans. Geosci. Rem. Sens.* 30, 356–369.
- Gerlein-Safdi, C., Gauthier, P.P., Caylor, K.K., 2018. Dew-induced transpiration suppression impacts the water and isotope balances of Colocasia leaves. *Oecologia* 187, 1041–1051.
- Gillespie, T., Brisco, B., Brown, R., Sofko, G., 1990. Radar detection of a dew event in wheat. *Rem. Sens. Environ.* 33, 151–156.
- Guerriero, L., Ferrazzoli, P., Vittucci, C., Rahmoune, R., Aurizzi, M., Mattioni, A., 2016. L-band passive and active signatures of vegetated soil: simulations with a unified model. *IEEE J. Sel. Top. Appl. Earth Obs. Rem. Sens.* 9, 2520–2531.
- Guerriero, L., Pierdicca, N., Pulvirenti, L., Ferrazzoli, P., 2013. Use of satellite radar bistatic measurements for crop monitoring: a simulation study on corn fields. *Rem. Sens.* 5, 864–890.
- Hamadi, A., Villard, L., Borderies, P., Albinet, C., Koleck, T., Le Toan, T., 2017. Comparative analysis of temporal decorrelation at P-band and low L-band frequencies using a tower-based scatterometer over a tropical forest. *Geosci. Rem. Sens. Lett. IEEE* 14, 1918–1922.
- Heffernan, S., Strimbu, B.M., 2021. Estimation of surface canopy water in Pacific Northwest forests by fusing radar, lidar, and meteorological data. *Forests* 12, 339.
- Herold, M., Pathe, C., Schmulius, C., 2001. The effect of free vegetation water on the multi-frequency and polarimetric radar backscatter—first results from the TerraDew 2000 campaign. In: *2001 IEEE International Geoscience and Remote Sensing Symposium (IGARSS)*, pp. 2445–2447. IEEE.
- Hornbuckle, B.K., Rowlandson, T.L., Russell, E., Kaleita, A., Logsdon, S., Kruger, A., Yueh, S., De Roo, R.D., 2010. How does dew affect L-band backscatter? Analysis of

- PALS data at the Iowa validation site and implications for SMAP. In: 2010 IEEE International Geoscience and Remote Sensing Symposium (IGARSS), pp. 4835–4838. IEEE.
- Huber, L., Gillespie, T., 1992. Modeling leaf wetness in relation to plant disease epidemiology. *Annu. Rev. Phytopathol.* 30, 553–577.
- Jang, M.y., Tien, K.J.C., Casanova, J., Judge, J., 2005. Measurements of soil surface roughness during the fourth microwave water and energy balance experiment: April 18 through June 13, 2005. Center Remote Sens., Univ. Florida, Gainesville, FL, USA. Tech. Rep. Circular 1483.
- Judge, J., Liu, P.W., Monsiváis-Huerta, A., Bongiovanni, T., Chakrabarti, S., Steele-Dunne, S.C., Preston, D., Allen, S., Bermejo, J.P., Rush, P., et al., 2021. Impact of vegetation water content information on soil moisture retrievals in agricultural regions: an analysis based on the SMAPVEX16-MicroWEX dataset. *Rem. Sens. Environ.* 265, 112623.
- Kabela, E.D., Hornbuckle, B.K., Cosh, M.H., Anderson, M.C., Gleason, M.L., 2009. Dew frequency, duration, amount, and distribution in corn and soybean during SMEX05. *Agric. For. Meteorol.* 149, 11–24.
- Karam, M., Fung, A., 1988. Electromagnetic scattering from a layer of finite length, randomly oriented, dielectric, circular cylinders over a rough interface with application to vegetation. *Int. J. Rem. Sens.* 9, 1109–1134.
- Khabbazan, S., Steele-Dunne, S., Vermunt, P., Judge, J., Vreugdenhil, M., Gao, G., 2021a. The influence of surface canopy water on the relationship between L-band backscatter and biophysical variables in agricultural monitoring. *Rem. Sens. Environ.* 268, 112789.
- Khabbazan, S., Vermunt, P.C., Steele-Dunne, S.C., Judge, J., 2021b. The importance of overpass time in agricultural applications of radar. In: 2021 IEEE International Geoscience and Remote Sensing Symposium (IGARSS), pp. 6084–6087. IEEE.
- Link, M., Entekhabi, D., Jagdhuber, T., Ferrazzoli, P., Guerriero, L., Baur, M., Ludwig, R., 2017. Simulating L/L-band and C/L-band active-passive microwave covariation of crops with the Tor Vergata scattering and emission model for a SMAP-Sentinel 1 combination. In: 2017 IEEE International Geoscience and Remote Sensing Symposium (IGARSS), pp. 4143–4146. IEEE.
- Liu, P.W., Judge, J., DeRoo, R., England, A., Luke, A., 2013. Utilizing complementarity of Active/Passive microwave observations at L-band for soil moisture studies in sandy soils. In: 2013 IEEE International Geoscience and Remote Sensing Symposium (IGARSS), pp. 743–746. IEEE.
- Liu, P.W., Judge, J., DeRoo, R.D., England, A.W., Bongiovanni, T., Luke, A., 2016. Dominant backscattering mechanisms at L-band during dynamic soil moisture conditions for sandy soils. *Rem. Sens. Environ.* 178, 104–112.
- Matzler, C., 1994. Microwave (1-100 GHz) dielectric model of leaves. *IEEE Trans. Geosci. Rem. Sens.* 32, 947–949.
- McNairn, H., Shang, J., 2016. A review of multitemporal Synthetic Aperture Radar (SAR) for crop monitoring. In: Ban, Y. (Ed.), *Multitemporal Remote Sensing*. Springer, Cham. Volume 20 of *Remote Sensing and Digital Image Processing* (chapter 15).
- METER Group, 2019. In: *Em50® Series Data Loggers from METER Group*. <https://www.metergroup.com/en/meter-environment/products/phytos-31-leaf-wetness-sensor>.
- METER Group, 2021a. In: *ECH2O EC-5 Moisture Sensor*. <https://www.metergroup.com/environment/products/ec-5-soil-moisture-sensor>.
- METER Group, 2021b. In: *PHYTOS 31 Dielectric Leaf Wetness Sensor*. <https://www.metergroup.com/en/meter-environment/products/phytos-31-leaf-wetness-sensor>.
- METER Group, 2021c. In: *Predicting the Amount of Water on the Surface of the PHYTOS 31 Dielectric Leaf Wetness Sensor*. <https://publications.metergroup.com/Sales%20and%20Support/METER%20Environment/Website%20Articles/predicting-amount-water-surface-lws-leaf-wetness-sensor.pdf>.
- Minh, D.H.T., Tebaldini, S., Rocca, F., Le Toan, T., Borderies, P., Kolecik, T., Albinet, C., Hamadi, A., Villard, L., 2014. Vertical structure of P-band temporal decorrelation at the Paracou forest: results from TropiScat. *Geosci. Rem. Sens. Lett. IEEE* 11, 1438–1442.
- Monteith, A.R., Ulander, L.M., 2021a. Temporal characteristics of P-band tomographic radar backscatter of a boreal forest. *IEEE J. Sel. Top. Appl. Earth Obs. Rem. Sens.* 14, 1967–1984.
- Monteith, A.R., Ulander, L.M., 2021b. A tower-based radar study of temporal coherence of a boreal forest at P-, L-, and C-bands and linear cross polarization. *IEEE Trans. Geosci. Rem. Sens.* 60, 1–15.
- Nagarajan, K., Liu, P.W., DeRoo, R., Judge, J., Akbar, R., Rush, P., Feagle, S., Preston, D., Terwilleger, R., 2013. Automated L-band radar system for sensing soil moisture at high temporal resolution. *Geosci. Rem. Sens. Lett. IEEE* 11, 504–508.
- Riedel, T., Pathe, C., Thiel, C., Herold, M., Schmullius, C., 2002. Systematic investigation on the effect of dew and interception on multifrequency and multipolarimetric radar backscatter signals. In: Wilson, A., Quegan, S. (Eds.), *Retrieval of Bio- and Geo-Physical Parameters from SAR Data for Land Applications*, vol. 475. ESA Special Publication, pp. 99–104. Provided by the SAO/NASA Astrophysics Data System.
- Riedel, T., Schmullius, C., 2003a. Effect of interception on the backscattering behaviour of crops. Provided by the SAO/NASA Astrophysics Data System Appl.SAR Polarim. *Polarimetr.Interferometr.ESA Special Publ.* 529, 71.1.
- Riedel, T., Schmullius, C., 2003b. Impact of interception on the thematic analyses of SAR data in agricultural areas. In: 2003 IEEE International Geoscience and Remote Sensing Symposium (IGARSS), pp. 2218–2220. IEEE.
- Stamenkovic, J., Ferrazzoli, P., Guerriero, L., Tuià, D., Thiran, J.P., Borgeaud, M., . Crop backscatter modeling and soil moisture estimation with support vector regression, in: 2014 IEEE Geoscience and Remote Sensing Symposium (IGARSS), IEEE. pp. 3228–3231.
- Steele-Dunne, S.C., McNairn, H., Monsiváis-Huerta, A., Judge, J., Liu, P.W., Papanthassiou, K., 2017. Radar remote sensing of agricultural canopies: a review. *IEEE J. Sel. Top. Appl. Earth Obs. Rem. Sens.* 10, 2249–2273.
- Tanase, M., Panciera, R., Lowell, K., Aponte, C., 2015. Monitoring live fuel moisture in semiarid environments using L-band radar data. *Int. J. Wildland Fire* 24, 560–572.
- Togliatti, K., Hartman, T., Walker, V.A., Arkebauer, T.J., Suyker, A.E., VanLoocke, A., Hornbuckle, B.K., 2019. Satellite L-band vegetation optical depth is directly proportional to crop water in the US Corn Belt. *Rem. Sens. Environ.* 233, 111378.
- Ulaby, F.T., El-Rayes, M.A., 1987. Microwave dielectric spectrum of vegetation-part ii: dual-dispersion model. *IEEE Trans. Geosci. Rem. Sens.* 550–557.
- Ulaby, F.T., Moore, R.K., Fung, A.K., 1981. *Microwave remote sensing: active and passive*. In: Volume 1-microwave Remote Sensing Fundamentals and Radiometry. Artech House, Boston.
- Ulander, L.M., Monteith, A.R., Soja, M.J., Eriksson, L.E., 2018. Multiport vector network analyzer radar for tomographic forest scattering measurements. *Geosci. Rem. Sens. Lett. IEEE* 15, 1897–1901.
- Vermunt, P.C., Khabbazan, S., Steele-Dunne, S.C., Judge, J., Monsiváis-Huerta, A., Guerriero, L., Liu, P.W., 2020. Response of subdaily L-Band backscatter to internal and surface canopy water dynamics. *IEEE Trans. Geosci. Rem. Sens.* 59, 7322–7337.
- Vermunt, P.C., Steele-Dunne, S.C., Khabbazan, S., Judge, J., van de Giesen, N.C., 2022a. Extrapolating continuous vegetation water content to understand sub-daily backscatter variations. *Hydrol. Earth Syst. Sci.* 26, 1223–1241.
- Vermunt, P.C., Steele-Dunne, S.C., Khabbazan, S., Kumar, V., Judge, J., 2022b. Towards understanding the influence of vertical water distribution on radar backscatter from vegetation using a multi-layer water cloud model. *Rem. Sens.* 14, 3867.
- Willis, A., 1984. Dune water and nutrient regimes—their ecological relevance. In: *Sand Dunes and Their Management: Report of a Meeting, Swansea, Focus on Nature Conservation*, pp. 159–174.
- Wood, D., McNairn, H., Brown, R., Dixon, R., 2002. Erratum to the effect of dew on the use of RADARSAT-1 for crop monitoring: choosing between ascending and descending orbits. *Rem. Sens. Environ.* 81, 456.
- Xu, X., Konings, A.G., Longo, M., Feldman, A., Xu, L., Saatchi, S., Wu, D., Wu, J., Moorcroft, P., 2021. Leaf surface water, not plant water stress, drives diurnal variation in tropical forest canopy water content. *New Phytol.* 231, 122–136.